THE DETERMINATION OF CRYSTAL POTENTIALS FROM HIGH ENERGY ELECTRON DIFFRACTION STUDIES ON MgO and Si

A Thesis
submitted in partial fulfillment of the
requirements for the degree of
Master of Science
at
The University of Manitoba

by
Alfonso Soler

May, 1970

© Alfonso Soler 1972

THE UNIVERSITY OF MANITOBA
ELIZABETH DAFOE LIBRARY

To
Antonio Soler
and
Carmen Gómez

TABLE OF CONTENTS

ACKNOWLEDGEMENTS

The author wishes to thank his advisor Dr. P. Gaunt of the Department of Physics for his interest and discussions throughout the development of this research.

The author would also like to thank Dr. K. Tangri and Dr. M.C. Chaturvedi of the Department of Materials Science for allowing him to use the electron microscope, and to Mr. J. van Dorpe for introducing him to the handling of the apparatus.

Appreciation is extended to Dr. J.M. Cowley of the University of Melbourne and Dr. P.S. Turner of the University of Oxford for useful private communications and Mrs. I. Hamel for her help in typing the thesis.

This work was supported by the National Research Council of Canada (Grant No. A5030).

INTRODUCTION

A determination of a crystal structure by means of x-ray diffraction is really a determination of the distribution of diffracting matter in a unit cell. At each point in the crystal, there is a certain density $\rho(x,y,z)$ of scattering matter, which is a function of the coordinates $(x,y,z) \equiv (\vec{r})$ of the point. The periodicity of a crystal structure allows us to write

$$\rho(x,y,z) = \sum_{G} \rho_{\vec{G}} e^{i \vec{r}\cdot\vec{G}} \qquad (1)$$

where $\vec{G}$ is a vector in the reciprocal lattice. The coefficients $\rho_{\vec{G}}$ are proportional to the x-ray structure factor $F_X(\vec{G})$. Absolute intensity measurements give values for the x-ray structure factors $|F_X(\vec{G})|$.

Let us now consider a high energy electron incident in a crystal. If we assume that it weakly perturbs the crystal lattice, the potential that the electron "sees" is just the potential determined by the periodicity of the lattice. This potential can be written

$$V(x,y,z) = \sum_{G} V_{\vec{G}} e^{i \vec{r}\cdot\vec{G}} \qquad (2)$$

The coefficients $V_{\vec{G}}$ are proportional to the electron structure factors $F_\theta(\vec{G})$. In the case of electron diffraction, intensity measurements will give information on the electron structure factor, and a determination of a crystal structure is really a determination of the crystal potential at each point in the crystal. If the assumption leading to (2) is

correct, a one to one correspondence can be established between x-ray and electron diffraction respectively, in the way

$$F_\theta(\vec{G}) \alpha (nZ - F_x(\vec{G})) \qquad (3)$$

where Z is the atomic number of the element considered and n the number of atoms per unit cell.

The interpretation of electron diffraction data is, in contrast with the x-ray case, in an early stage of development. Experimental intensity data can be analyzed with two different theories, the Kinematical and the Dynamical.

In the Kinematical Theory, two waves are considered, one transmitted and one diffracted. The amplitude of the incident wave is taken as constant, and it is assumed that the diffracted intensity is small in comparison with the transmitted. The theory leads to the conclusion that the diffracted intensity can exceed the incident intensity at the Bragg peak, for a certain thickness of the crystal observed (less than 100 Å for many materials). For crystals frequently used in electron microscopy, where the thickness can reach values of 1000 Å, the results of the Kinematical Theory cannot be trusted.

The Dynamical Theory takes into account the possible dynamical interactions of incident and scattered waves. Its simplest form is the two beam theory, where only the transmitted and one diffracted beam are considered.

The many beam Dynamical Theory, takes into account the possible existence of many diffracted waves, unavoidable in practice, as can be seen by observing any diffraction pattern

in the electron microscope.

The parameter extinction distance is defined as twice the distance in the crystal for a diffracted wave to build up to unit amplitude, and can be determined by many beam theory and experimentally by observation of thickness fringes in electron microscope images of wedge crystals.

The value of the extinction distance depends on the V_G's, Fourier coefficients of the crystal potential. These coefficients can be derived from values of the electron structure factors, calculated for the free atom by Hartree-Fock or Thomas-Fermi-Dirac methods. But in a crystal, bonding effects are important, and the wave functions of the outer-most electrons in the atom will be modified relative to those appropriate for the free atoms. Fortunately, the influence of the outer-most electrons in the structure factor is only strong for low order reflections, and for high order reflections, free atom calculations are fairly accurate.

A fitting method has been developed that allows a refinement of low order structure factors by comparison of many beam theoretical, and experimental extinction distances.

In chapters one, two three and four, the Dynamical Theory is introduced giving, when possible, original derivations. In chapter five, the fitting method is described and applied to the calculation of V_{200} and V_{400} for MgO. Results are compared with other electron diffraction and x-ray data available, and the validity of a two beam theory is discussed. Chapter six is devoted to the study for MgO of

CHAPTER I

1.1 Need for a Dynamical Theory of Electron Diffraction

Two theories have been developed for electron diffraction studies, the Kinematical and the Dynamical. In the Kinematical Theory, the amplitude of the incident wave is taken as constant, and thus it is assumed that the diffracted intensity is small in comparison with the transmitted. Expressions for diffracted amplitude at the bottom of the crystal being considered are written simply by adding up the amplitudes of the waves scattered by individual atoms, taking due account of the phase without considering the possibility of subsequent scattering of the diffracted waves by other atoms. The failure of the Kinematical Theory becomes serious for small deviations from positions of exact Bragg reflection for the crystal considered. The Theory leads to the conclusion that near the Bragg peak, diffracted intensities can exceed the incident intensities for a certain thickness of the crystal observed. The critical thickness at which the Kinematical Theory is no longer valid for 100 KeV - usual energy of the electrons incident in the crystal - has been estimated as about 15 Å for the 111 reflection of Au and similarly for other materials.

For the crystals used in Electron Microscopy, where thickness can reach values of 1000 Å, and observations at the Bragg peak are required, the results of the Kinematical Theory cannot be trusted, and it is necessary to devise an improved

leaf 2 omitted
in page numbering.

Theory, the Dynamical Theory, taking into account the dynamical interactions of incident and scattered waves.

CHAPTER II

2.1 Quantum Mechanical Formulation of the Dynamical Theory.

The principles of the Dynamical Theory have been well established in the study of electron diffraction, since it was inaugurated by Bethe [1], as well as done by Ewald [2] and Laue [3] for x-ray diffraction.

In the Dynamical Theory, the Schrödinger equation for an electron incident in a crystal is solved under appropriate boundary conditions, by assuming the wave function for the electron to be a superposition of plane waves, and the potential energy determined by the periodicity of the lattice.

The Schrödinger equation for an electron incident in a crystal plus the crystal can be written

$$\left\{-\frac{h^2}{2m}\nabla^2 + H_c + V(r)e\right\} (\vec{r},\vec{r}_1\ldots\vec{r}_n) = E^1 e\ (\vec{r},\vec{r}_1\ldots\vec{r}_n) \qquad (1)$$

where $-\frac{h^2}{2m}\nabla^2$ represents the kinetic energy of the incident electron, H_c is the crystal Hamiltonian, and $V(\vec{r})$ describes the interaction of the incident electron and the crystal. In (1), $\vec{r}$ is used for the incident electron and $\vec{r}_1\ldots\vec{r}_n$ for the electrons in the crystal.

The plasma frequency for different materials lies in the range of 10^{15} to 10^{16} seconds^{-1}. The time that takes an incident 100kv electron to traverse a unit cell of a material with a lattice parameter of the order of 5 Å is of the order

of 10^{-18} seconds. It appears to be very unlikely that collective excitations will take place. As a consequence the state of the crystal can be regarded as independent of the incident electron and we can write

$$\Psi(\vec{r},\vec{r}_1 \ldots \vec{r}_n) = a(\vec{r}_1 \vec{r}_2 \ldots \vec{r}_n)\ \psi\ (\vec{r}) \qquad (2)$$

where a is the wave function representing the stage of the crystal and ψ describes the elastic scattering of the incident electron.

Equation (1) now becomes

$$H_c a = e\varepsilon a \qquad (3a)$$

$$\left(V(r) - \frac{\hbar^2}{2m} \nabla^2\right) \psi = Ee\psi \qquad (3b)$$

where Ee is the total energy of the incident electron in electron volts and $e\varepsilon$ corresponds to the electrons in the lattice.

In practice, energy losses of the order 20 eV for incident energies of 100keV are observed [4], and (2) should be regarded as an approximation.

2.2 Nature of the Crystal Potential Seen by the Incident Electron. Basic Equation of the Dynamical Theory.

We are now concerned with the solution of equation (3b). We have assumed that the incident electron does not perturb the crystal lattice, so, we can assume that the potential $V(\vec{r})$ that the incident electron "sees" is just the potential determined by the periodicity of the lattice when we consider the crystal isolated. If this assumption

is correct to a good approximation, one to one correspondence between data for $\rho(\vec{r})$ as determined by x-ray experiments and for $V(\vec{r})$ as determined by electron diffraction can be established.

Let $V(\vec{r}) = V(xyz)$ be the potential at $\vec{r}$ in the lattice the axis of the crystal being parallel to the primitive translations a,b,c of the lattice. The structure of the crystal is periodic parallel to x,y,z in the distances a,b,c respectively. The crystal potential at any point $(x,0,0)$ must be expressible by a Fourier series of the type

$$V(\vec{r}) = \sum_h V_{h,o,o} \text{ cosin } (hx/a) \tag{4}$$

where h,o,o are Miller indexes.

Considering the periodicity parallel to y and z, we can write

$$V(\vec{r}) = \sum_{-\infty}^{\infty}\sum\sum V(h,k,l)e^{+ i (\frac{hx}{a} + \frac{ky}{b} + \frac{lz}{c})} \tag{5}$$

This formula can be written in reciprocal lattice formalism. If $\vec{r}$ is the vector from the origin to the point (x,y,z) and $\vec{G}$ is the vector to the point (h,k,l) of the reciprocal lattice, perpendicular to the plane (h,k,l)

$$\vec{G}\cdot\vec{r} = \frac{hx}{a} + \frac{ky}{b} + \frac{z}{c}$$

and as a consequence,

$$V(\vec{r}) = \sum_{\vec{G}} V_{\vec{G}}\, e^{\, i\, \vec{r}\cdot\vec{G}} = \sum_G \frac{\hbar^2}{2me} U_{\vec{G}}\, e^{\, i\, \vec{G}\cdot\vec{r}} \tag{6}$$

where we have written for convenience,

$$V_{\vec{G}} = \frac{\hbar^2}{2me} U_{\vec{G}} \tag{7}$$

Since $V(\vec{r})$ is real, and we assume $V(\vec{r}) = V(-\vec{r})$

$$U_G = U_{-G} = U_G^*$$

Now we look for a general solution of equation (3b) of the type

$$\psi_k(\vec{r}) = \sum_G C_{\vec{k}+\vec{G}}\, e^{\,i(\vec{k}+\vec{G})\vec{r}} \qquad (8)$$

where C_{G+k} are constants, and $\vec{G}$ is a reciprocal lattice vector. This is a Bloch wave as

$$\psi_R(\vec{r}) = \sum_G C_{k+G}\, e^{\,i(\vec{k}+\vec{G})r} = e^{\,i\vec{k}\vec{r}} \sum_G C_{k+G}\, e^{i\vec{G}\vec{r}} = e^{\,i\vec{k}\vec{r}}\, u_k \qquad (9)$$

and u_k is periodic.

Substituting in equation (3b) equations (6) and (8) and operating we obtain

$$\left(\frac{2mE}{\hbar^2} - (\vec{K}+\vec{G})^2\right) C_G + \sum_h U_h\, C_{G-h} = 0 \qquad (10)$$

This is the basic equation for the Dynamical Theory of electron diffraction. We have used a non relativistic Schrödinger's equation, but relativistic effects are important because of the high energies of the incident electrons.

Fujiwara [5] was able to show that the relativistic effects can be adequately described by using equation (10) if the elementary relativistic corrections for the electron mass and wavelength are performed.

CHAPTER III

3.1 The Two Beam Approximation.

It is not difficult to develop equation (10) in the special case of systematic reflections, that is when a row of reciprocal lattice points $n\vec{g}$, for $n = 0 \pm 1 \pm 2...$ is close to the Ewald sphere where $\vec{g}$ is the reciprocal lattice vector for the reflection of lowest order considered. Nevertheless, the wave mechanical equation (10) is usually solved in its approximate form, that assumes that only two strong beams, one incident and the other diffracted are excited in the crystal.

In the reflecting sphere construction, this is equivalent to assuming that only one reciprocal lattice point lies near the sphere.

Although this is a very reasonable assumption in the case of x-ray diffraction, where the radius of the reflecting sphere λ^{-1} is small, for electron diffraction, with values for λ^{-1} of the order of 27 $\mathring{A}$ for 100 keV, many lattice points lie close to the sphere, and precaution should be taken when interpreting experimental results with a two beam theory.

We shall take as non zero the intensities for the transmitted beam ($h = 0$) and the first diffracted beam ($h = 1$). In this way, equation (10) is equivalent to the system

$$(K^2 - k^2)\ C_o(\vec{k}) + U_{-g}\ C_g(\vec{k}) = 0 \qquad (11)$$

$$U_g\, C_o(k) + (K^2 - (\vec{k}+\vec{g})^2)\, C_g(k) = 0 \qquad (11)$$

where we have written $C_g(k)$ for C_{g+k} and $K^2 = \frac{2mEe}{\hbar^2} + U_o$

A solution of (11) exists if

$$\begin{vmatrix} K^2 - k^2 & U_{-g} \\ U_g & K^2 - (\vec{k}+\vec{g})^2 \end{vmatrix} = 0 \qquad (12)$$

that is if

$$(k^2 - K^2)\,(|\vec{k}+\vec{g}|^2 - K^2) - U_g U_{-g} = 0 \qquad (13)$$

In equation (12) knowing the value of U_o, the total energy of the incident electron eE, the value of U_g, the mass of the electron relativistically corrected and Planck's constant, we can solve for k.

Equations of the type (13) which relate the wave vector to the energy are called dispersion equations, and restrict the wave vector to lie on some kind of surface called dispersion surface.

If we give a two dimensional representation to $\vec{k}$, that is we assume that it has two components, k_x parallel to $\vec{g}$, and k_z perpendicular to $\vec{g}$,

$$\vec{k}^2 = k_x^2 + k_z^2$$

and

$$|\vec{k} + \vec{g}|^2 = k_x^2 + k_z^2 + 2k_x\vec{g} + \vec{g}^2 \qquad (14)$$

When we are at the Bragg peak for the reflection at $\vec{g}$

$$|\vec{k}| = |\vec{k} + \vec{g}|$$

thus

$$|k_x| = g/2$$

In general, if we fix k_x in equation (13) we can solve for k_z and we will obtain two possible values of k_z for each value of the incident energy. For $K = 27$ $\mathring{A}^{-1}$ corresponding to 100 keV and $U_o = U_g = 0.058$ $\mathring{A}^{-2}$, with $g = 0.476$ $\mathring{A}^{-1}$ we have plotted in figure 1, continuous line, the corresponding dispersion surface k_x versus k_z. The dotted line corresponds to a different value of U_g, $U_o = U_g = 0.053$ $\mathring{A}^{-2}$. It is evident that the separation of the two branches of the dispersion surface has changed appreciably.

We shall call the two solutions for a certain value of the incident energy and a fixed value of $\vec{k}$, $\vec{k}^{(1)}$ and $\vec{k}^{(2)}$; let $\vec{k}^{(1)} > \vec{k}^{(2)}$. The construction we have given in figure 1 presuposes that the two waves excited in the crystal have the same k_x component. This is because of the classical boundary condition of constant derivative of the wave function at the top of the crystal $(z = 0)$. On the other hand it is interesting to note that the two excited waves have different kinetic energies. As the total energy of the electron is conserved, a difference in kinetic energy corresponds to a difference in potential energy. It appears reasonable then, to suppose that the wave with higher $\vec{k}$ will spend more time in the regions of low potential energy, near the atoms in the crystal and as a consequence, it is scattered more.

Figure 1. Two beam dispersion surfaces in the first Brillouin zone, for two different values of U_g at 100 keV.

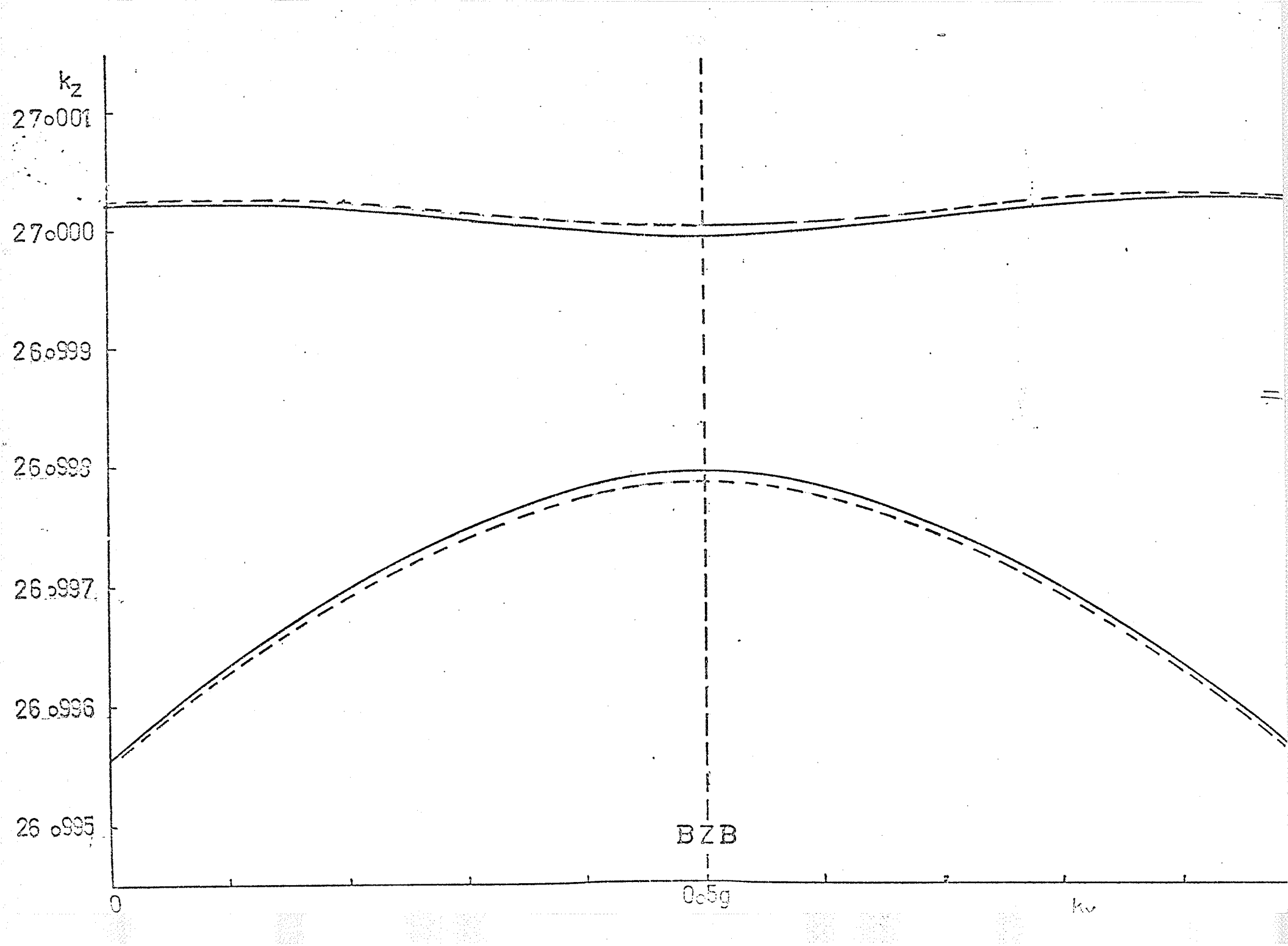
k_z
27.001
27.000
26.999
26.998
26.997
26.996
26.995
BZB
0
0.5g
k_x

3.2 The Wave Vector Gap in the Two Beam Dispersion Surface. Correspondence with the Energy Gap in Band Theory.

We should like now to come back to equation (3a) for the electrons in the crystal, that we had separated from equation (3b) for the incoming electron.

If the interaction between electrons in the crystal is weak

$$a(\vec{r}_1 \ldots \vec{r}_n) = a(\vec{r}_1)\ a(\vec{r}_2) \ldots\ a(\vec{r}_m) \tag{15}$$

so that for $a(\vec{r}_i) = a_i$ equation (3a) becomes

$$\begin{aligned} H_{c_1} a_1 &= e\varepsilon_1 a_1 \\ H_{c_2} a &= a\varepsilon_2 a_2 \\ \ldots &= \ldots \end{aligned} \tag{16}$$

Every Schrödinger equation in (16) is identical with the one we have solved for the incoming electron. The only difference is the much lower energy of the electrons already in the metal.

Solutions for the energy of the electron eE, if $\vec{k}$ varies along a certain direction are studied in energy band theory. It is well known from the nearly free ($\equiv$ two beam) electron model that at the Bragg peak, an energy gap of the value $2V_g e$ takes place. We should like to present a discussion of the kind of corresponding gap in the dispersion surface treatment as outlined in 3.1. A perfect analogy between band theory and electron diffraction dispersion surfaces can be made only in the case of low

energy electron diffraction [6].

In figure 2, it is clear that the vector $\vec{k}$ can be expressed as

$$\vec{k} = [(\frac{g}{2} - k_{11}), o, k_z]$$

where $g/2 - k_{11}$ is the component parallel to the vector $\vec{g}$ considered and k_z is the perpendicular component.

Substituting in equation (13) and making $U_o = 0$,

$$\left(eE - \frac{\hbar^2}{2m} \{(\vec{g}/2)^2 + k_{11}^2 + k_z^2\} - \frac{\hbar^2}{2m} k_{11} g\right)$$

$$\left(eE - \frac{\hbar^2}{2m} \{(\vec{g}/2)^2 + k_{11}^2 + k_z^2\} + \frac{\hbar^2}{2m} k_{11} g\right) = |V_g e|^2 \qquad (17)$$

and

$$Ee = \frac{\hbar^2}{2m} \left((g/2)^2 + k_z^2 + k_{11}^2\right) \pm \sqrt{|V_g e|^2 + \{\frac{\hbar^2}{2m} k_{11} g\}} \qquad (18)$$

At the Bragg peak $k_{11} = 0$. As a consequence, possible solutions for the energy are

$$\begin{aligned} Ee &= A_{kz} + C \\ Ee &= A_{kz} - C \end{aligned} \qquad (19)$$

where A is

$$\frac{\hbar^2}{2m} \left((g/2)^2 + k_z^2\right) \qquad (20a)$$

and C is

$$\sqrt{|V_g e|^2} = |V_g e| \qquad (20b)$$

In the dispersion surface approach, for two different values of k_z, $k_z^{(1)}$ and $k_z^{(2)}$ corresponding to the same $k_{11} = 0$, we must take

$$eE_{k^{(1)}} - eE_{k^{(2)}} = 0 = \frac{\hbar^2}{2m} (k_z^{(1)2} - k_z^{(2)2}) + 2V_g e \qquad (21)$$

Figure 2. Decomposition of a wave vector $\vec{k}$ in the first Brillouin zone.

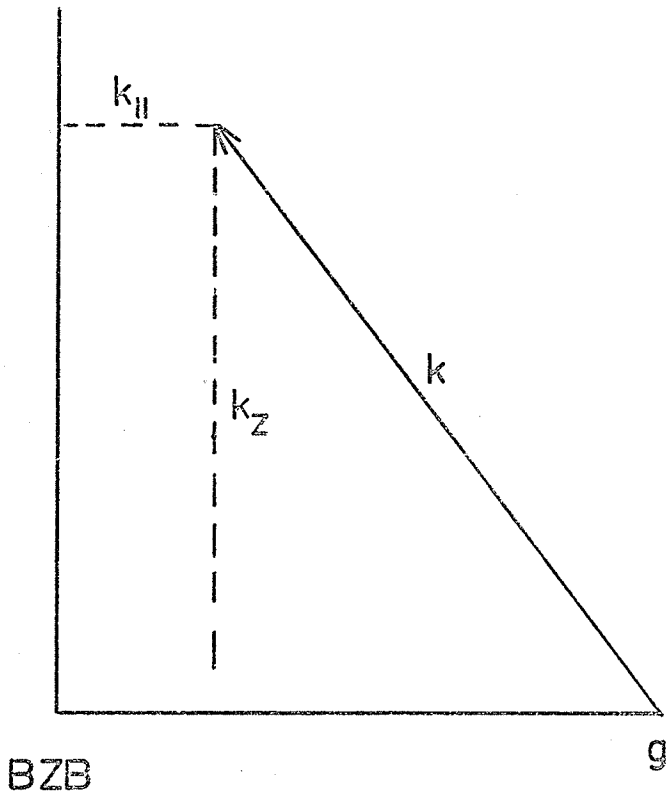
$k_{\parallel}$
k_z
k
BZB
g

and if we set $k_z^{(1)} \simeq k_z^{(2)} \simeq K$, the distance $k_z^{(1)} - k_z^{(2)}$ in the dispersion surface becomes using equation (13)

$$\Delta k_z = k_z^{(2)} - k_z^{(1)} \simeq \frac{2V_g e \hbar^2}{(2m)(2K)} = \frac{U_g}{K} \tag{22}$$

As we mentioned before, in band theory we are interested in studying different values of the energy of the electrons in the crystal for fixed values of k along a certain direction. At the Bragg peak, if we suppose this direction in the x-z plane, for a certain value $k_{11} = 0$, we have two different energies. As a consequence we take

$$\begin{aligned} eE_1 &= A_{k_{z_1}} + C \\ eE_2 &= A_{k_{z_1}} - C \end{aligned} \tag{23}$$

or

$$eE_1 - eE_2 = 2V_g e \tag{24}$$

The energy band diagram and the constant energy dispersion surface of the dynamical theory are in fact sections of the same hypersurface with the appropriate constraint surface. In figure 3, we have plotted a three dimensional view of the dispersion hypersurface in the first Brillouin zone together with the trace (near the Brillouin zone boundary) of the surface (dbc^1f^1) on a plane of constant energy $E_1 e$ and the trace $(abcf)$ on a plane of arbitrary $\vec{k}$ = constant (Stern et al. [6]).

Both planes contain the common point b that lies on the edge of the gap (common for both the dispersion surface and the energy band scheme). Transversing the gap at constant $\vec{k}$ (from b to c) is not equivalent to transversing it from

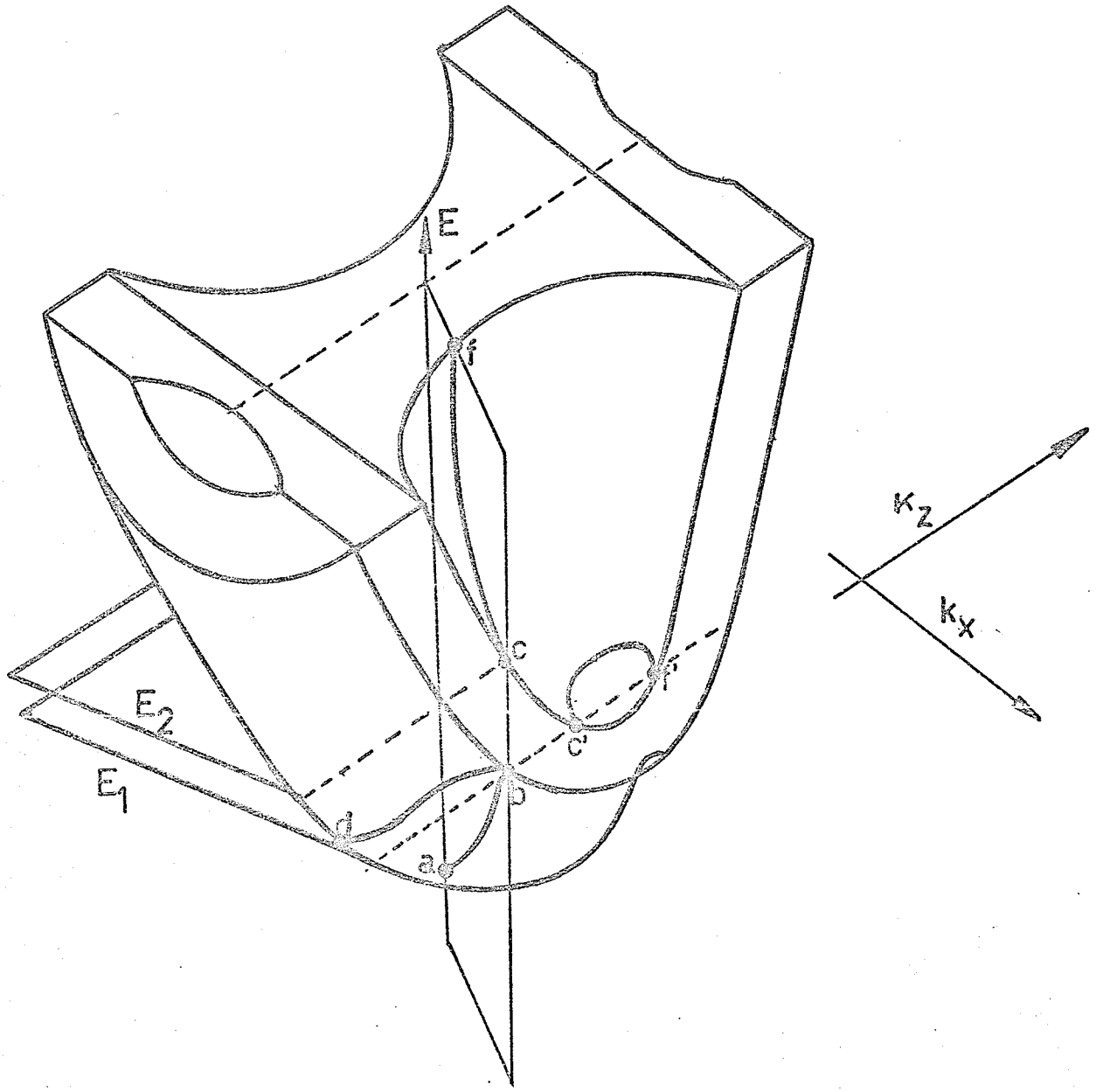

THREE DIMENSIONAL ISOMETRICAL VIEW OF THE DISPERSION HYPERSURFACE IN THE FIRST BRILLOUIN ZONE

(After Stern et al Ref. 6)

b to c[1] (at constant energy). In fact, from b to c, the value of k_z changes from $k_z^{(1)}$ to $k_z^{(2)}$.

3.3 Diffracted Intensity in Two Beam Theory

To find the amplitude for the diffracted wave corresponding to the $n\vec{g}$ reflection (n = 0,1 for a two beam case) we have to take into account each of the wave functions for different branches of the dispersion surface (two branches in the two beam case), with certain amplitudes that we shall call α_i, where i refers to the branch considered.

Thus, in general, for the $n\vec{g}$ row of systematic reflections

$$\psi_{n\vec{g}} = \sum_i \alpha_i C_{n\vec{g}}^{(i)} \exp\left(i\left(\vec{k}^{(i)}+n\vec{g}\right)\vec{r}\right) \qquad (25)$$

where $\vec{k}^{(i)} + n\vec{g}$ is the wave vector for the n reflection in the ith branch, that we shall write $k_{n\vec{g}}^{(i)}$. Our problem is to find $\psi_{n\vec{g}}$.

If we imagine waves incident in the surface of the foil, let the amplitudes of the waves be represented by $u_{n\vec{g}}^{(i)}$ corresponding to branch i. This is merely a formal device to handle the matching of the incident and transmitted and diffracted waves at the top of the foil. In fact we only have one incident, one transmitted and many diffracted waves (one in the two beam case). At the top of the crystal using:

$$\alpha_i C_{n\vec{g}}^{(i)} = u_{n\vec{g}}^{(i)} \qquad (26)$$

then

$$\sum_i u_{n\vec{g}}^{(i)} = \sum_i \alpha_i C_{n\vec{g}}^{(i)} = \psi_{n\vec{g},o}\left(\vec{r} = o\right) \qquad (27)$$

Multiplying both sides of equation (26) by $C^{*j}_{\vec{ng}}$

$$\alpha_i \, C^{(i)}_{\vec{ng}} C^{(j)*}_{\vec{ng}} = u^{(i)}_{\vec{ng}} \, C^{(j)*}_{\vec{ng}} \tag{28}$$

and summing up with index ng

$$\sum_{ng} \alpha_i \, C^{(i)}_{\vec{ng}} C^{(j)*}_{\vec{ng}} = \sum_{ng} u^{(i)}_{\vec{ng}} C^{(j)*}_{\vec{ng}} \tag{29}$$

The left hand side of equation (28) is, if the orthogonality condition $\sum_{\vec{ng}} C^{(i)}_{\vec{ng}} \, C^{(j)*}_{\vec{ng}} = 0 \ (i \neq j), = 1 (i = j)$ holds

$$\sum_{ng} \alpha_i \, C^{(i)}_{\vec{ng}} \, C^{x(j)}_{\vec{ng}} = \alpha_{i = j} \tag{30}$$

In this way, equation (28) becomes

$$\alpha_i = \sum_{ng} u^{(i)}_{\vec{ng}} \, C^{(j)*}_{\vec{ng}} \tag{31}$$

Only $u^{(i)}_{\vec{ng}} = 1$ if $n = 0$, so that only one term $(n = 0)$ exists in equation (30). Thus

$$\alpha_i = u^{(i)}_{o} \, C^{(i)*}_{ng} = C^{(i)*}_{o} \tag{32}$$

and equation (27) is now

$$1 = \Sigma \, u^{(i)}_{ng} = C^{(1)\,2}_{o} + C^{(2)\,2}_{o} + C^{(3)\,2}_{o} + \ldots \tag{33}$$

where 1 is the value of the incident intensity, and only the first two terms of the right hand side exist in a two beam theory.

With (32), (25) becomes

$$\psi_{\vec{ng}} = \sum_{i} C^{(i)*}_{o} \, C^{(i)}_{\vec{ng}} \exp \left(i \, \vec{k}^{(i)}_{\vec{ng}} \, \vec{r}\right) \tag{34}$$

We are interested in this section in the diffracted intensity $|\psi_g|^2$ in two beam theory. In figure 4, we introduce $\vec{s}_o$ and $\vec{s}_g$ as deviations from the Bragg condition $(s_o = 0)$ and $\zeta^{(i)}$, $i = 1,2$ as distance from $D^{(i)}$ on the

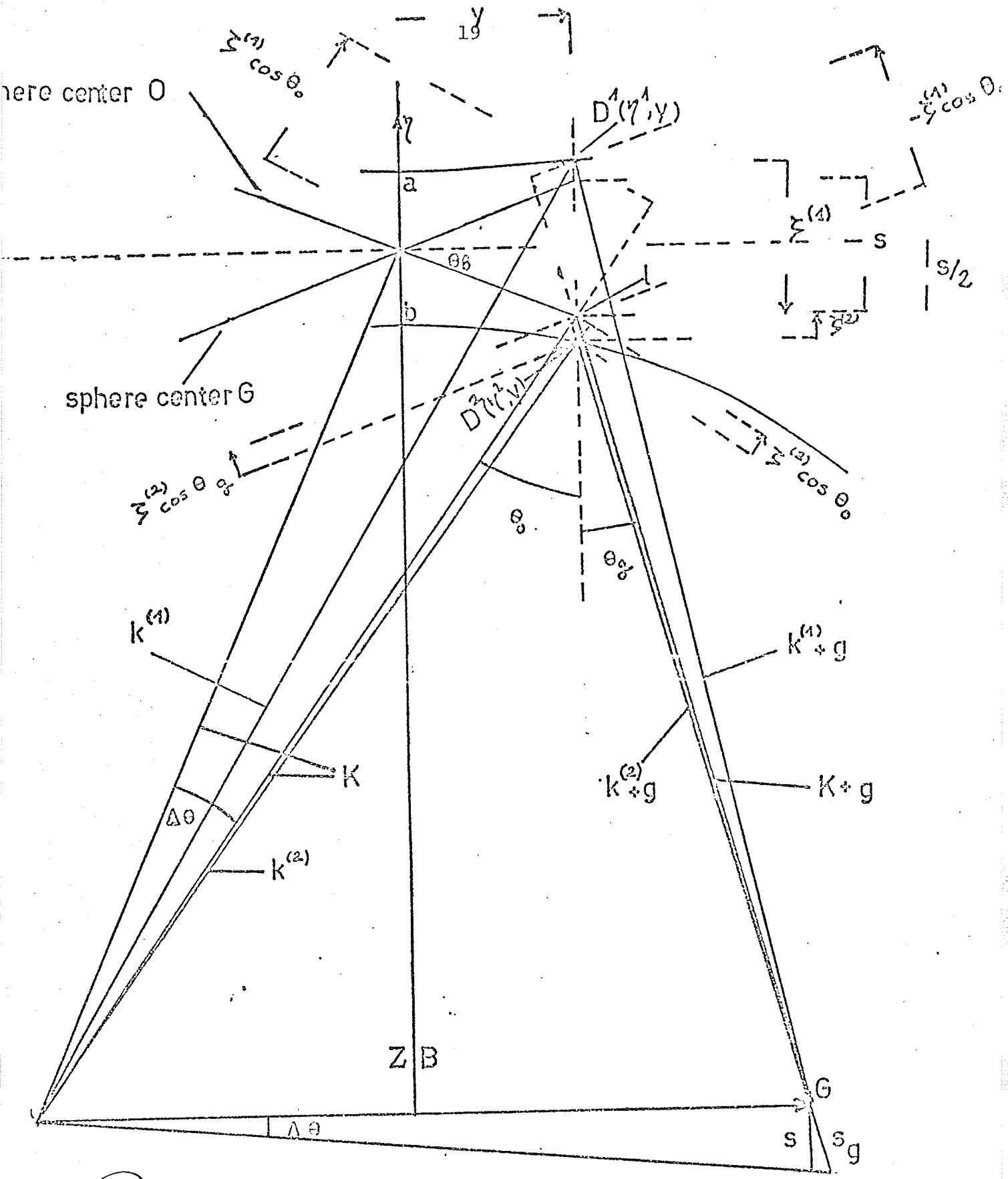

DISPERSION SURFACE (TWO BEAM) (see text)

i branch of the dispersion surface to the corresponding point 1 in the sphere of radius $\vec{K}$. Through 1 we draw a line normal to the vector $\vec{g}$ considered. This line through 1 and $D^{(i)}$ will be parallel to the zone boundary (BZB).

From figure 4 it is clear that

$$\vec{K}^{(i)} = K - \vec{s}_{ng} - \vec{\zeta}^{(i)} \cos \theta_{ng} \tag{35}$$

and if we assume $\cos\theta_{ng} = 1$, writing $K - \vec{s}_{ng} = \vec{H}_{ng}$, (34) becomes

$$\psi_{ng} = \sum_i C_o^{(i)} C_{ng}^{(i)*} \exp (i \zeta^{(i)} z) \exp (i \vec{H}_{ng} \vec{r}) \tag{36}$$

The intensity for the $\vec{g}$ reflection for our two beam case will be

$$|\psi_g|^2 = |\sum_{i=1,2} C_o^{(i)*} C_g^{(i)} \exp (-i \zeta^{(i)} z)|^2 \tag{37}$$

The formalism can be in general extended to many beams by considering other values of i.

3.4 Extinction Distances in Two Beam Theory.

Equation (36) was first derived by Fujimoto [7]. We shall now arrive by an original treatment to the determination of the parameter extinction distance to be defined later.

For a perfect understanding of this section, figure 4 is absolutely necessary. In figure 4 a point in any of the branches of the dispersion surface considered, $D^{(i)}$ has coordinates (η_i, y_i). We observe

$$\cos \theta_B = \frac{y}{1D^{(1)}} \tag{38}$$

and

$$\text{tg } \Delta\theta = \left(\frac{y}{\cos\theta_B}\right) K \tag{39}$$

From the Ewald sphere construction

$$\text{tg } \Delta\theta = s/g \tag{40}$$

where s is the projection on the axis perpendicular to $\vec{g}$ of the deviation from the Bragg condition (bottom of the figure). Using the Bragg condition

$$g = 2K\sin\theta_B \tag{41}$$

we obtain the important relation

$$2y \text{ tg } \theta_B = s \tag{42}$$

If we consider points $D^{(i)}$ very close to the zone boundary (for a clear understanding of the limitations of equation 43 as derived from this condition see figure 1)

$$\eta^{(1)} = -\eta^{(2)} \tag{43}$$

and

$$\zeta^{(1)} = \zeta = (\eta^{(1)}+\frac{s}{2}) \tag{44}$$

$$\zeta^{(2)} = -(\eta^{(1)}-\frac{s}{2}) \tag{45}$$

To find the value of $\eta^{(1)}$ we see in figure 4 that

$$\vec{k}^{(2)}-\vec{K} = (\eta^{(2)}+y \text{ tg } \theta_B)\cos\theta_B \tag{46}$$

$$|\vec{k}^{(2)}+\vec{g}|-\vec{K} = (\eta^{(2)}- y \text{ tg } \theta_B)\cos\theta_B \tag{47}$$

and because of (43)

$$\vec{k}^{(2)}-K = -(|\vec{k}^{(1)}+\vec{g}|-K) \tag{48}$$

$$|\vec{k}^{(2)}+\vec{g}| -K = -(\vec{k}^{(1)}-K) \tag{49}$$

From equation (12) and if $k_z^{(1)} \simeq k_z^{(2)} \simeq K$, with $\cos\theta_B = 1$

$$(\eta - y \text{ tg } \theta_B)(\eta + y \text{ tg}\theta_B) = \frac{U_g^2}{4K^2} \tag{50}$$

With the help of equation (42) and our original derivation of the wave vector gap at the Bragg peak in equation (22), equation (50) gives

$$\eta = \tfrac{1}{2}\sqrt{s^2+(\Delta k)^2} \tag{51}$$

One of the boundary conditions for an electron in a beam incident in a crystal, is that for no penetration $(z = \bar{0})$ there is no diffracted beam. Thus, in equation (37)

$$[C_o^{(1)*} C_g^{(1)}] = -[C_o^{(2)*} C_g^{(2)}] \tag{52}$$

Taking equations (51), (44), (45) into account

$$I_g = |\psi g|^2 = |C_o^{(1)*} C_g^{(1)}|^2 \; |e^{-i(\frac{1}{2}\sqrt{s^2+(\Delta k)^2}+\frac{s}{2})z} \; e^{i(\frac{1}{2}\sqrt{s^2+(\Delta k)^2}-\frac{s}{2})z}|^2$$

Operating

$$I_g = |C_o^{(1)*} C_g^{(1)}|^2 \; |(2i)^2 \sin^2(\frac{z}{2}(\Delta k)(s^2(\Delta k)^{-2}+1)^{\frac{1}{2}})| \tag{54}$$

This is the usual result obtained by wave optical, Darwin like theory [9], but now derived in quite an easy way. On the other hand, we note that because of the approximation involved, equation (54) is valid only for certain distances from the zone boundary.

The parameter extinction distance, defined in two beam theory at the Bragg peak as twice the distance in the crystal that must contribute for the diffracted beam to build up to maximum amplitude, is immediately derived from equation (54).

At the Bragg peak, for the $\vec{g}$ reflection $s = 0$ and (54) reduces to

$$I_g = |C_o^{(1)} * C_g^{(1)}|^2 \; |-2i \sin(\Delta k)\frac{z}{2}|^2 \qquad (55)$$

The distance that must contribute for the diffracted beam to build up to maximum amplitude is

$$z = \frac{1}{2(\Delta k)} \qquad (56)$$

The extinction distance ε_g, is by definition twice the distance in equation (56), so that

$$\varepsilon_g = \frac{1}{\Delta k} = \frac{K}{U_g} \qquad (57)$$

and (55) becomes

$$|\psi g|^2 = |2i\, C_o^{(1)} * C_g^{(1)}|^2 \sin^2\left(\frac{z}{2}\,\varepsilon_g^{-1}\,\sqrt{s^2\varepsilon^2+1}\,\right) \qquad (58)$$

From equation (58), it is clear that I_g will ocillate with depth in the crystal, with a periodicity $\varepsilon_g/\sqrt{(\varepsilon_g s)^2 + 1} = \varepsilon_g(s)$ giving rise to thickness fringes in a wedge crystal. At the Bragg peak (s = 0), the spacing of the fringes seen in electron microscope images of wedge crystals can give us, if a two beam theory is applicable, the extinction distance, that can be compared with the value of equation (57).

CHAPTER IV

4.1 Many Beam Theory.

In Chapter III of this thesis, we have studied the two beam theory for the transmitted and first diffracted beam in the crystal. In general, a two beam theory gives $\varepsilon_{ng}(s)$ when the transmitted and ng diffracted beam are taken into account. When in the fifties, experiments with thickness fringes began, it was usually assumed, that the experimental extinction distances were in good agreement with a two beam theory. As we have mentioned before, the two beam case is impossible in practice, where the simultaneous reflections ng for n:-4... 4.. are unavoidable. In the sixties, the development of the many beam theory has given a powerful weapon to compare experimental results with theoretical conclusions.

We shall briefly indicate how the many beam calculations have been performed in this thesis. We have used a nine beam theory, that is, we have taken into account the transmitted and eight diffracted beams. It was tested that to take more beams into account didn't influence our final conclusions.

By simple inspection of equation (10), the nine beam case can be expressed for a centrosymetric crystal, for the ng set of simultaneous reflections:

$$\begin{vmatrix} H_0 & U_1 & U_1 & U_2 & U_2 & U_3 & U_3 & U_4 & U_4 \\ U_1 & H_1 & U_2 & U_1 & U_3 & U_2 & U_4 & U_3 & U_5 \\ U_1 & U_2 & H_{-1} & U_3 & U_1 & U_4 & U_2 & U_5 & U_3 \\ U_2 & U_1 & U_3 & H_2 & U_4 & U_3 & U_5 & U_2 & U_6 \\ U_2 & U_3 & U_1 & U_4 & H_{-2} & U_5 & U_1 & U_6 & U_2 \\ U_3 & U_2 & U_4 & U_1 & U_5 & H_3 & U_6 & U_1 & U_7 \\ U_3 & U_4 & U_2 & U_5 & U_1 & U_6 & H_{-3} & U_7 & U_1 \\ U_4 & U_3 & U_5 & U_2 & U_6 & U_1 & U_7 & H_4 & U_8 \\ U_4 & U_5 & U_3 & U_6 & U_2 & U_7 & U_1 & U_8 & H_{-4} \end{vmatrix} \begin{vmatrix} C_0 \\ C_1 \\ C_{-1} \\ C_2 \\ C_{-2} \\ C_3 \\ C_{-3} \\ C_4 \\ C_{-4} \end{vmatrix} = 0 \qquad (59)$$

where C_{ng} and U_{ng} have been abbreviated to C_n and U_n and $H_n = K^2 - (\vec{k}+n\vec{g})^2$.

For the two beam case, the geometry of the situation shows that the diagonal elements of the matrix, for the reflection mg at the exact Bragg position are given by [8]

$$H_n = K^2 - k_z^2 - \left(\frac{m}{2} - n\right)^2 g^2 \qquad (60)$$

The same equation can be proved to be correct for a many beam case.

Being k_z unknown in (59), our general objective is to solve the many beam equation (59) for k_z^2 leading to $k_z^{(1)}$ $k_z^{(2)} \ldots k_z^{(9)}$ and to find

$$C = \begin{vmatrix} C_0^{(1)} & \ldots & C_0^{(i)} & \ldots & C_0^{(9)} \\ C_1^{(1)} & \ldots & C_1^{(i)} & \ldots & C_1^{(9)} \\ \cdot & \cdot & \cdot & \cdot & \cdot \\ C_{-4}^{(1)} & \ldots & C_{-4}^{(i)} & \ldots & C_{-4}^{(9)} \end{vmatrix} \qquad (61)$$

where the ith column of C is the Bloch wave on the ith branch of the 9 beam dispersion surface.

What we want is as a consequence, to find the eigenvalues and eigenvectors of the matrix

$$\begin{vmatrix} Q_0 & U_1 & \cdots & & \\ U_1 & & & & \\ \cdot & & & & \\ \cdot & & & & \\ \cdot & & & & \\ \cdot & & & & \\ \cdot & & & & \\ U_{+4} & \cdots & \cdots & & Q_{-4} \end{vmatrix} \qquad (62)$$

where $Q_n = H_n + k_z^2 = K^2 - \left(\frac{m}{2} - n\right)^2 g^2$.

To do so, we must first of all determine all the elements of the matrix. Let us first consider the Fourier coefficients of the crystal potential. They are usually calculated from electron scattering amplitudes because there are tables for such amplitudes easily available. The formula used is

$$F_\theta\ (h',\ k',\ l') = \frac{2\pi m_0 e}{h^2\ V_c}\ V_{h'k'l'} \qquad (63)$$

where $V_{h'k'l'}$ is the Fourier coefficient of the crystal potential, $F_\theta(h',k',l')$ is the electron structure factor, related to the electron scattering amplitude in the same way that for the x-ray case (where we talk about x-ray scattering factors and x-ray structure factor), e is the charge of the electron, m_o its mass, h Planck's constant, and V_c the volume of the unit cell. This formula is demonstrated in Appendix I.

The relation between $V_{h',\ k',\ l'}$ and $U_{h',\ k',\ l'}$

was given in (7). If relativistic effects are taken into account, we obtain the following formula to calculate the U's in the matrix

$$U_{h,k,l} = \frac{F_\theta(h,k,l)}{\pi V_c \sqrt{1-\frac{v^2}{c^2}}} \qquad (64)$$

where F_θ is as in (63) the non-relativistic structure factor, v is the velocity of the incident electron, and c the velocity of light. For the volume of the unit cell in $\mathring{A}^3$, $U_{h,k,l}$ comes given in $\mathring{A}^{-2}$.

We see that $U_{h,k,l}$ will increase with the accelerating voltage, but $V_{h,k,l}$ will remain independent of the voltage as it should be.

To determine the elements of the diagonal of the matrix, we must determine K and U_0. As $K^2 >> U_0$, U_0 has not been included in the calculations. To determine K, the following relation determined from relativistic considerations has been used

$$K = \lambda^{-1} = \frac{\left(2m_0 Ee\left[1+\frac{eE}{2m_0 c^2}\right]\right)^{\frac{1}{2}}}{h} \qquad (65)$$

where eE is the kinetic energy of the incident electron (total energy inside of the crystal), m_0 the rest mass of the electron, c the velocity of light and h Planck's constant.

Substituting numerical values, the following useful relation is found [9]

$$K = \frac{E^{\frac{1}{2}}(1 + 0.9788.10^{-6}E)}{12.26} \qquad (66)$$

where E is measured in volts.

A computer programme based on the "Eigen" sub-routine of IBM has been devised to calculate the eigen values and eigen vectors of (62) and is shown in Appendix IIa. A programme specifically written for the 9 beam case is given in Appendix IIb.

The programming for the data input to the standard sub-routine (EIGEN) has been written by the author in Fortran IV (360).

Figure 5 shows a 9 beam dispersion surface (only the first seven branches are seen) calculated for the {200} set of systematic reflections of MgO. The values of U_g, U_{2g}, etc. are given in Table 1, (see section 5.3 of the thesis) with $K = 27.02\ \mathring{A}^{-1}$ and $g = 0.475\ \mathring{A}^{-1}$. In the rest of Chapter IV we shall be concerned with the {200} row of systematic reflections for MgO.

4.2 Extinction Distances in Many Beam Theory

In the nine beam theory outlined in 4.1 we have seen that for a fixed k_x, there will be nine column vectors which satisfy equation (59), each corresponding to a Bloch wave with a particular value of k_z, denoted by $k_z^{(i)}$ (we take $k_z^{(1)}$ $k_z^{(2)} \ldots k_z^{(9)}$) and belonging to one of the nine branches of the dispersion surface shown in Figure 5. A linear combination of all nine Bloch waves will be excited in the crystal, so that the resultant effect can be in principle quite complicated. We are now interested in relating experimental values of thickness fringes spacings as observed in wedge crystals to the values that we can obtain using

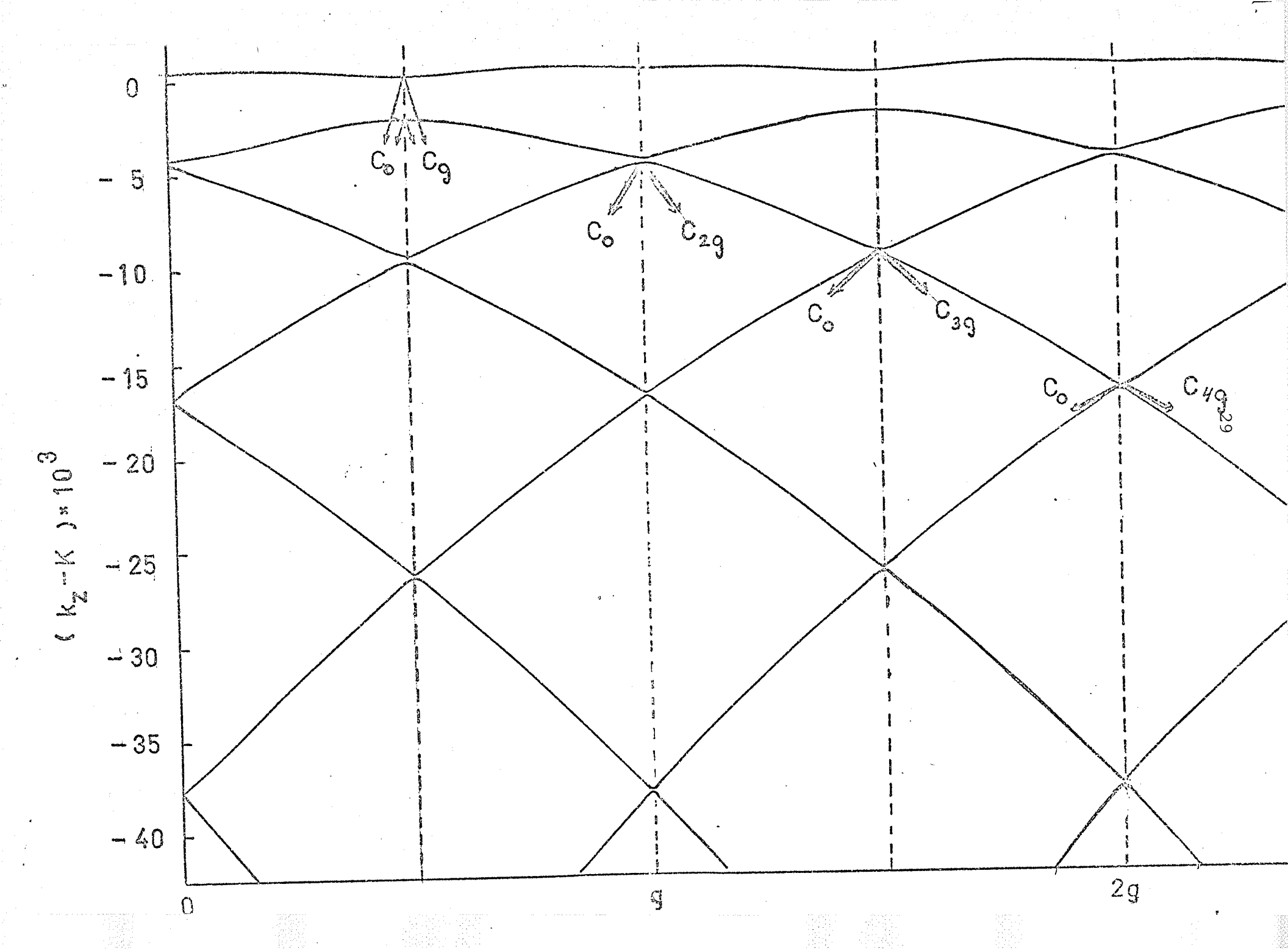
0
- 5
- 10
- 15
- 20
- 25
- 30
- 35
- 40
(k_z - K) × 10^3
C_o
C_g
C_o
C_{2g}
C_o
C_{3g}
C_o
C_{4g}
0
g
2g

many beam theory.

It has been proved recently [14], that for a four beam case, the value $|k_z^{(1)} - k_z^{(2)}|^{-1}$, where $k_z^{(1)}$ and $k_z^{(2)}$ correspond to the Bloch waves with largest intensities $|C_o^{(1)}|^2$ and $|C_o^{(2)}|^2$ (see formula 33), gives a periodicity for the diffracted intensity I_{200} corresponding to equation (55) with the 200 reflection at the Bragg peak, only if the intensity minimae are taken into account. That is, if we measure spacings between intensity minimae, we can compare them with $|k_z^{(1)} - k_z^{(2)}|^{-1}$ as indicated in 4.1.

Although detailed calculations have not been done yet for a larger number of beams, it is likely that conclusions will be similar. The procedure can obviously be extended to ε_{400}, ε_{600} etc. In general, wave vectors $k_z^{(i)}$, $k_z^{(j)}$, corresponding to the largest intensities $|C_o^{(i)}|^2$ $|C_o^{(j)}|^2$ will give $|k_z^{(i)} - k_z^{(j)}|^{-1}$ as many beam extinction distance corresponding to the Bragg peak considered.

We have applied the preceeding ideas to the {200} row of systematic reflections of MgO and found that

$$\varepsilon_{200} = |k_z^{(1)} - k_z^{(2)}|^{-1} \text{ for 200 at the Bragg peak}$$
$$\varepsilon_{400} = |k_z^{(2)\prime} - k_z^{(3)\prime}|^{-1} \text{ for 400 at the Bragg peak}$$
$$\varepsilon_{600} = |k_z^{(3)\prime\prime} - k_z^{(4)\prime\prime}|^{-1} \text{ for 600 at the Bragg peak}$$
$$\ldots \qquad \ldots$$

At the same time, we shall talk of $\varepsilon_{200}(s) = |k_z^{(1)\prime} - k_z^{(2)\prime}|^{-1}$ as of the 200 extinction distance with 400 at the Bragg peak, or in general of values of the 200 extinction distance for the 200 reflection out of the Bragg

peak in correspondence with the ideas developed in the two beam case (see 3.3).

4.3 Object of the Thesis.

The only problem left to compare experimental and many beam theory values of extinction distances is to introduce in matrix (62) the adequate values of the Fourier coefficients of the crystal potential. This implies accurate knowledge of the corresponding electron scattering amplitudes. These amplitudes can be calculated assuming atoms in the crystal to be free atoms, by Hartree-Fock and Thomas-Fermi-Dirac techniques [15]. But in a crystal, bonding effects are important, and the wave functions of the outer electrons will be modified relative to those appropriate to the free atom. This leads to inaccuracies of the order of 20% or more in the evaluation of electron scattering amplitudes for low order reflections (e.g. 200), and as a consequence, to inaccuracies in the corresponding Fourier coefficients of the crystal potential.

The main purpose of this thesis is to find the real coefficients of the crystal potential by fitting many beam theoretical values of extinction distances to experimental values, as determined by observation of thickness fringes in wedge crystals. Fortunately, the influence of the outer most electrons in the structure factors is only large for low order reflections and for high order reflections (e.g. 600), free atom calculations are fairly accurate.

CHAPTER V

5.1 Description of the Fitting Method Used.

In Chapter V of this thesis, we shall consider the set of systematic reflections for MgO. It is obvious that each of the extinction distances ε_{200}, ε_{400} etc., as defined in Chapter IV depends in a different way on the Fourier coefficients of the crystal potential U_{200}, U_{400} etc. ε_{200} will depend strongly on U_{200} and less on U_{400}, U_{600} ... because the reflection 200 is now at the Bragg peak. The extinction distance ε_{400} will strongly depend on U_{400} and less on U_{200} and U_{600}. At the same time the influence of U_{600} will be larger on ε_{400} than on ε_{200}, because the 600 reflection is closer to the 400 than to the 200. The other extinction distances can be looked at with the same arguments. Thus the following fitting method is suggested.

If we know the experimental value of ε_{200}, we can vary U_{200} in the many beam matrix till the theoretical ε_{200} fits the experimental ε_{200}. We shall call U'_{200} the new value of U_{200}. With this new value U'_{200} substituted in the matrix corresponding to the 400 reflection at the Bragg peak U_{400} can be varied till ε_{400} fits the experimental ε_{400}. We call U'_{400} the new value of U_{400}. Now U'_{200} and U'_{400} are substituted in the many beam matrix for 600 at the Bragg peak, and U_{600} is varied till ε_{600} agrees with the experimental ε_{600}. In this way, U'_{600} is determined. The method can be extended to modifications of

the potentials U_{800} U_{1000} etc., by considering the many beam matrixes for 800, 1000, etc. at the Bragg peak.

The potentials U'_{200}, U'_{400}, U'_{600}, U'_{800}... obtained in this way seem to be a better approach to the real ones. to obtain more accurate values, the whole process must be repeated as many times as necessary. That is, now we repeat the same treatment but beginning with U'_{200}, U'_{400}, U'_{600}... instead of the original U_{200}, U_{400}, U_{600}... . In this way we obtain U''_{200}, U''_{400}, U''_{600}, ... Further repitition will give U'''_{200}, U'''_{400}, U'''_{600} ... if we begin with U''_{200}, U''_{400}, U''_{600}... etc.

A perfect convergence for the proposed method has been found. Clearly the main advantage is that the method is systematic. The success of this method in the determination of real x-ray scattering factors could seem surprising if we take into account that a point by point intensity fitting has been suggested as absolutely necessary by Pollard and Turner [16]. Further on, the method is simplified by the fact that absorption effects need not be included to a very good approximation as tested by the author (for an understanding of absorption effects and an elementary treatment see Chapter VIII). A method based in fitting of intensities should take the anomalous absorption effect into account, and only theoretically determined crystal potentials are usually available [46].

5.2 Experimental Data Available for MgO.

To apply the procedure outlined in 5.1, experimental extinction distances for the 200, 400, 600, ... reflections for MgO should be available. Uyeda and Nonoyama [17] (to be referred as UN in the future) have studied ε_{200} for 100 keV electrons. Their conclusion is that a two beam theory is explanatory of the variation of ε_{200} with deviation from the Bragg peak. Dupoy et al. [18] (to be referred to as D in the future) have measured ε_{200} for different voltages, from 100 to 1200 keV. They have concluded that a two beam theory is not explanatory of their results for energies higher than 300 keV.

Finally Uyeda [19] (to be referred to as U in the future) has determined ratios $\frac{\varepsilon_{400}}{\varepsilon_{200}}$ at 100, 200, 350 and 500 keV by direct measurement of distances between maximae and minimae of intensity in photographs of thickness fringes, in an attempt to confirm the validity of Bethe's second approximation, a two beam theory in which the two beam potential includes many beam effects. As the results did not fit the theory, he decided they were in error of 20% or more because of inaccuracy in extinction distance determination with direct measurements on photographs. He has also given experimental results for the variation of ε_{200} with deviation from the Bragg peak at 100 keV and 500 keV, and the variation of ε_{400} with 400 at the Bragg peak, for 100, 200, 350 and 500 keV. (UN) have given after eight months of measurements ε_{200} = 456±7Å at 100 keV, D a value of 446±7Å at the same voltage.

U has given $\frac{\varepsilon_{400}}{\varepsilon_{200}} = 3.26$ at 100 keV. The experimental values have been plotted in figures 8, 9, 10 and 11.

5.3 Determination of V_{200} and V_{400} for MgO.

Experimental values of ε_{600}, ε_{800} ... are not available. Thus we are faced with limiting our fitting method to ε_{200} and ε_{400}. We shall comment later on the influence of assuming the theoretical values of U_{600}, U_{800} ... as the correct ones.

As in his paper, U only gives values of $\varepsilon_{400}/\varepsilon_{200}$ his value $\varepsilon_{400}/\varepsilon_{200} = 3.26$ at 100 keV was applied to ε_{200} = 446, 449, 463, 456 and 440Å, and thus, possible experimental values of ε_{400} were supposed to be 1454, 1464, 1511, 1488 and 1434Å.

The fitting method was applied with the initial values of the relativistic potentials listed in Table I. They were determined by application of (64) with electron scattering factors taken from the International Tables of X-ray Crystallography [20].

TABLE I

$k = 27\text{Å}^{-1}$	$g = 0.475\text{Å}^{-1}$
Energy	= 100 keV
U_{200}	$= 0.0583\ \text{Å}^{-2}$
U_{400}	$= 0.02627\text{Å}^{-2}$
U_{600}	$= 0.01456\text{Å}^{-2}$
U_{800}	$= 0.00869\text{Å}^{-2}$
U_{1000}	$= 0.00586\text{Å}^{-2}$
U_{1200}	$= 0.00450\text{Å}^{-2}$
U_{1400}	$= 0.00397\text{Å}^{-2}$

These potentials are for a temperature of 0°K, and will be used to fit experimental data supposedly at 20°C. If our fitting method is consistent, fitted results for U_{200}, U_{400} will be the same for the same U_{600}, U_{800}, ..., independently of the initial values of U_{200} and U_{400}. A correction must be applied to the final values of U_{200} and U_{400} due to the fact of assuming U_{600}, U_{800} ... at 0°K.

For the exactitude of the fitting method, interpolation between two values of U_{2h00} differing in as much as 10^{-3} $\mathring{A}^{-2}$ was done in the first steps assuming a linear dependence between U_{200} and $1/\varepsilon_{200}$, U_{400} and $1/\varepsilon_{400}$. The linearity has been proved to be certain in a two beam theory (see Chapter III of this thesis). It was confirmed that linearity persists in the many beam case, from 100 to 1000 keV for variations of U_{200} and U_{400} of a maximum of 0.1 $\mathring{A}^{-2}$, that is in fact larger than the potentials themselves. In figure 6 we have given the variation of $1/\varepsilon_{200}$ with U_{200} U_{400} and U_{600} for 100 keV electrons, and the direction of the variation of $1/\varepsilon_{200}$ with U_{200}, U_{400} and U_{600} for 900 keV electrons* (broken line). The linearity indicates that when U_{200} or U_{400} or U_{600} vary, $1/\varepsilon_{200} = \alpha U_{200} + \beta$ or $\alpha' U_{400} + \beta'$ or $\alpha'' U_{600} + \beta''$. Similar relations were seen to take place with U_{800}, U_{1000} etc. In the figure, it is clear that for a certain variation of ε_{200} the required variation of U_{200} is smaller than that of U_{400} in agreement with the ideas in 5.1.

*values of k and $\frac{v}{c}$ for voltages different from 100 keV are listed in Appendix IV of reference 9.

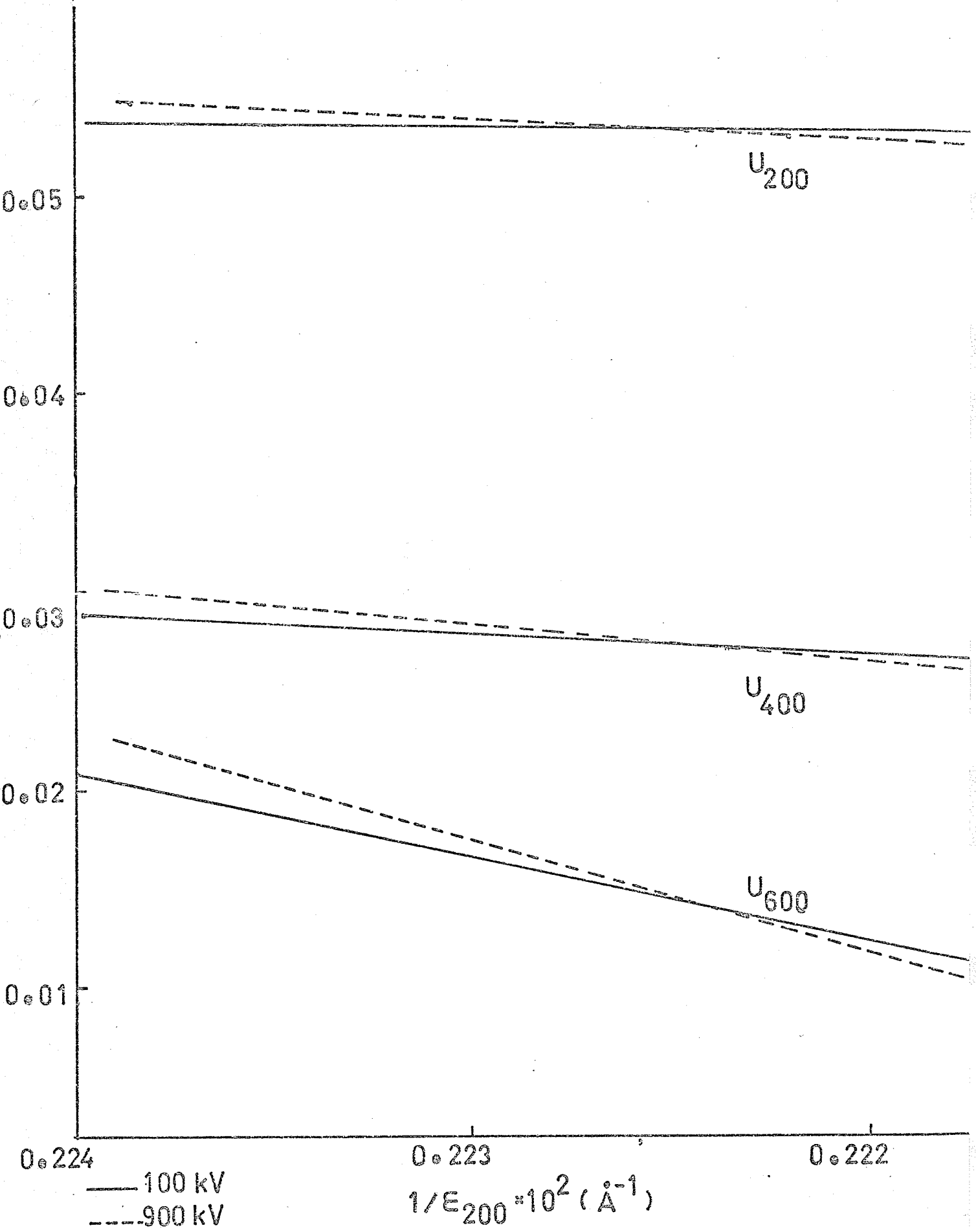
0.05
0.04
0.03
0.02
0.01
U_{200}
U_{400}
U_{600}
0.224
0.223
0.222
100 kV
900 kV
$1/E_{200} \cdot 10^2$ (Å^{-1})

In figure 7 we have plotted $1/\varepsilon_{400}$ versus U_{200} U_{400} , U_{600} for keV electrons, and the direction of $1/\varepsilon_{400}$ versus U_{200} , U_{400} , U_{600} at 900 keV. This time $1/\varepsilon_{400}$ $= \gamma U_{200} + \delta = \gamma' U_{400} + \delta' = \gamma'' U_{600} + \delta''$, and for a certain variation of ε_{400} , the required variation of U_{400} is smaller than that of U_{200} than that of U_{600} .

Let us immediately say that the method proved to be convergent. As an example, we give in table II, for a 456-1488 Å fitting ($\varepsilon_{400}/\varepsilon_{200} = 3.26$ at 100 keV) the results for U'_{200} , U'_{400} , U''_{200} , U''_{400} , U'''_{200} , ... It was not necessary to obtain U^{v}_{200} , U^{v}_{400} ... as the convergence is fast.

TABLE II

$U'_{200} = 0.05278$ Å^{-2}	$U'''_{200} = 0.05220$ Å^{-2}
$U'_{400} = 0.02984$ Å^{-2}	$U'''_{400} = 0.02960$ Å^{-2}
$U''_{200} = 0.05207$ Å^{-2}	$U^{v}_{200} = 0.05216$ Å^{-2}
$U''_{400} = 0.02936$ Å^{-2}	$U^{v}_{400} = 0.02945$ Å^{-2}

The final value for U'_{200} of 0.0522 Å^{-2} and the value for U'_{400} of 0.0294 Å^{-2} are clearly nonsense when compared with corresponding results obtained from available theoretical or experimental information (see 5.4). For 463-1511 Å, values of $U'_{200} = 0.0515$ Å^{-2} and of $U'_{400} = 0.0285$ Å^{-2} were obtained. These are also clearly nonsense when compared with other available results.

Values of $\frac{\varepsilon_{400}}{\varepsilon_{200}}$ for 200, 300, 400 and 500 keV were calculated for U_{200} and U_{400} as determined by the 456-1488 Å, the 463-1511 Å and the 440-1434 Å fittings (these values at 100 keV). The resultant curve for the 459-1488 Å

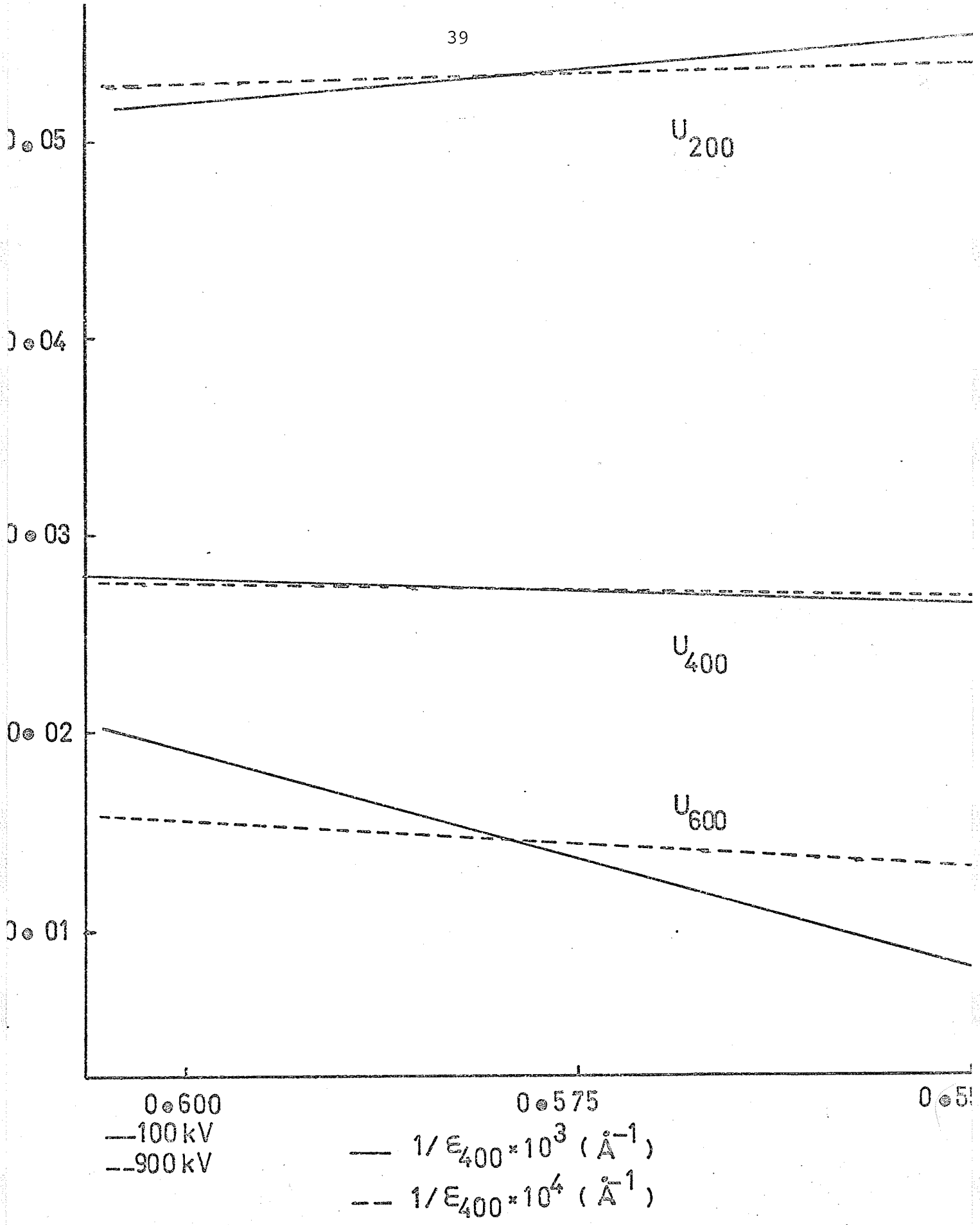
0.05
0.04
0.03
0.02
0.01
U_{200}
U_{400}
U_{600}
0.600
0.575
0.5
—100 kV
--900 kV
— $1/\varepsilon_{400} \times 10^3$ ($Å^{-1}$)
--- $1/\varepsilon_{400} \times 10^4$ ($Å^{-1}$)

fit is the lowest in figure 8. As it is seen, the whole curve lies far from the experimental values (circles) given by U, for energies higher than 100 keV.

It seemed interesting to repeat the fitting with different values of $\frac{\varepsilon_{400}}{\varepsilon_{200}}$ at 100 keV. This was done for values of $\frac{\varepsilon_{400}}{\varepsilon_{200}}$ = 3.4, 3.6, 3.8 and 4, for ε_{200} = 446, 456, 463 Å. In figure 8 we have plotted the results for $\frac{\varepsilon_{400}}{\varepsilon_{200}}$ = 3.6 and 3.85* (at 100 keV from 100 to 500 keV.) Results for the 3.85 fitting are for ε_{200} = 456 Å and are regarded as best fit. Results for $\frac{\varepsilon_{400}}{\varepsilon_{200}}$ = 3.6 are also for ε_{200} = 456 Å. Values of U_{200}^{IV} and U_{400}^{IV} are given in Table III for different values of $\frac{\varepsilon_{400}}{\varepsilon_{200}}$. The values for the 3.85 fit are especially marked.

TABLE III

	446	456	463	
U_{200}^{IV}	0.0534	0.0525	0.0518	3.6
U_{400}^{IV}	0.0287	0.0278	0.0272	
U_{200}^{IV}	0.0537	0.0527	0.0520	3.8
U_{400}^{IV}	0.0279	0.0270	0.0264	
($Å^{-2}$) U_{200}^{IV}	0.0537(5)	0.0528(5)	0.0520(5)	3.85 $\frac{\varepsilon_{400}}{\varepsilon_{200}}$
U_{400}^{IV}	0.0277	0.0273	0.0262	
U_{200}^{IV}	0.0539	0.0529	0.0522	4
U_{400}^{IV}	0.0271	0.0262	0.0256	

In the following sections $U^{IV} = U$ to facilitate the discussion. We note that the values of U_{200} and U_{400} have been determined using values of U_{600}, U_{800}, etc. at 0°K. If values of U_{600}, U_{800} are corrected for temperature,

*At this point results were obtained by interpolation, given the almost perfect periodicities in Table III.

it is likely that the values in Table III will change. Ohtsuki [21] has demonstrated that the temperature dependence of V_{hkl} can be described in a satisfactory way by multiplying the 0°K potential (corresponding to a 0°K election scattering amplitude) by the corresponding Debye-Waller factor $\exp(-B\frac{\sin^2\theta}{\lambda^2})$.

The value of B was not determined in any of the experiments mentioned and we have taken $B = .215$ Å, in order to compare in the next section our results with x-ray results for which $B_{Mg} = 0.24$ Å and $B_O = 0.19$ Å were experimentally determined.

In this way, values for U_{600}, U_{800} ... were determined at 100 keV in substitution of the values in Table I (for 0°K) and are listed in Table IV.

TABLE IV

U_{400}	0.0130 Å^{-2}
U_{600}	0.0071 Å^{-2}
U_{800}	0.0042 Å^{-2}
U_{1000}	0.0029 Å^{-2}
U_{1200}	0.0021 Å^{-2}

The fitting for $\frac{\varepsilon_{400}}{\varepsilon_{200}} = 3.85$ at 100 keV was repeated again and the values obtained for U_{200} and U_{400} where the ones in Table III but shifted by $\sim+ 10^{-4}$Å^{-2} and $\sim+ 5.10^{-4}$ Å^{-2} respectively. The shift should be larger if larger values for B are considered.

Thus, for $\varepsilon_{200} = 456$ Å we get for the 3.85 fit

$U_{200} \sim 0.0528 \mathring{A}^{-2}$ and $U_{400} \sim 0.0273 \mathring{A}^{-2}$. If an error of $\pm$ 10 $\mathring{A}$ is assumed in ε_{200}, final values of U_{200} and U_{400} are $U_{200} = 0.0528 \pm 10\ \mathring{A}^{-2}$, and $U_{400} = 0.0273 \pm 10\ \mathring{A}^{-2}$. These values also cover a possible error of $\pm$ 0.15 in the determination of the best value of $\frac{\varepsilon_{400}}{\varepsilon_{200}}$ at 100 keV. We observe nevertheless, that the higher we go in values for the ratio $\frac{\varepsilon_{400}}{\varepsilon_{200}}$, U_{200} and U_{400} vary in opposite sense, but they vary in the same sense for a shift in extinction distance for the same value of the ratio.

Values for V_{200} and V_{400} as obtained with formula (63) were derived from the values of U_{200} and U_{400} given the the preceeding paragraph and are given in Table V.

TABLE V

V_{200}	V_{400}	
6.63 $\pm$ 0.12	3.42 $\pm$ 0.12	volts

These values are consistent, that is are independent of the initial values of U_{200} and U_{400}. This was tested for initial values of U_{200} and U_{400} different from those in Table I but using the same values for U_{600}, U_{800} ... of Table I, taking $\varepsilon_{200} = 456\ \mathring{A}$.

We wish to remark that although the possible error in ε_{200} has been taken as $\pm$10 $\mathring{A}$, a minimum experimental error of $\pm$7 $\mathring{A}$ has always been achieved. Such an error gives values of the x-ray scattering factor for the first reflection with an error of 0.5%, that places the method within the most precise available for x-ray scattering factor determination.

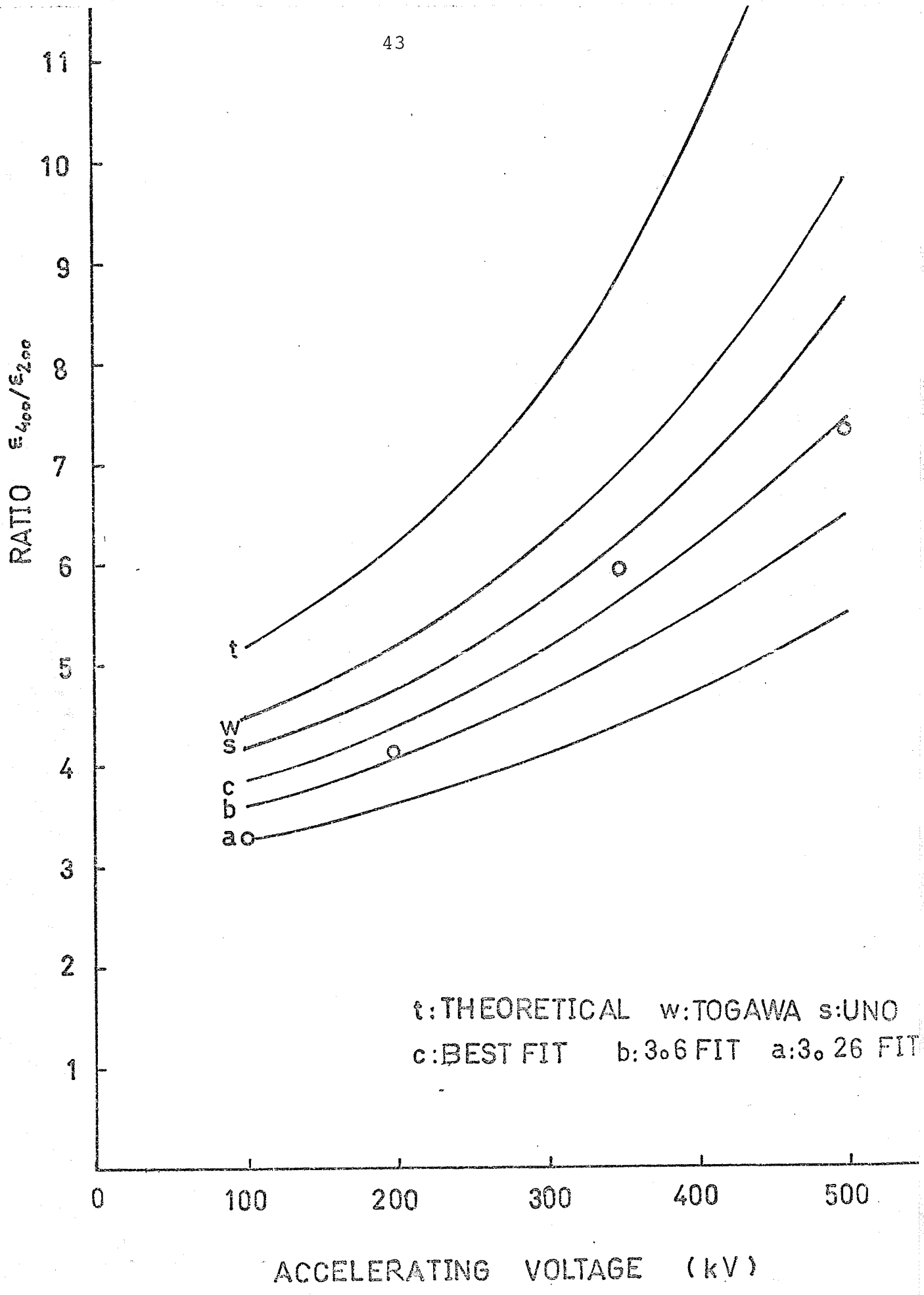
RATIO $\varepsilon_{400}/\varepsilon_{200}$
11
10
9
8
7
6
5
4
3
2
1
0
100
200
300
400
500
ACCELERATING VOLTAGE (kV)
t
w
s
c
b
a
t:THEORETICAL w:TOGAWA s:UNO
c:BEST FIT b:3.6 FIT a:3.26 FIT

It is also interesting to point out that if more careful experimental measurements of $\frac{\varepsilon_{400}}{\varepsilon_{200}}$ are done in the future, the error of ± 0.15 for the value of the best fit at 100 keV is from our point of view excessive.

5.4 Analysis of the Results

Results already available for V_{200} and V_{400} are of three types: x-ray experimental determinations, in the form of x-ray scattering factors, electron diffraction data in the form of crystal potentials, and theoretical data as obtained by Hartree-Fock or more detailed techniques.

The relation between x-ray scattering factors and electron scattering amplitudes ($f_x(h,k,l)$ and $f_\theta(h,k,l)$) is provided by Poisson's equation. If the potential distribution can be separated into additive contributions from individual atoms x-ray scattering factors may be derived from the Mott formula

$$f_\theta = \frac{m_0 e^2}{2h^2} \quad \frac{(Z-f_x)}{p^2} \tag{67}$$

where $p = \frac{\sin\theta}{\lambda}$ and Z is the atomic number of the element. This relation is valid at 0°K.

It has been theoretically determined [27] that if at a certain temperature the observed value of the x-ray scattering factor obtained in an x-ray experiment is $f_x\, e^{-B\,\frac{\sin^2\theta}{\lambda^2}}$ the corresponding value of the electron scattering factor to be observed in an electron diffraction experiment (as determined from the experimental crystal potential) is at the same

temperature $f_\theta\, e^{-B\frac{\sin^2\theta}{\lambda}}$, that is,

$$f_{el}\, e^{-B\frac{\sin^2\theta}{\lambda^2}} \rightarrow f_x\, e^{-B\frac{\sin^2\theta}{\lambda^2}} \qquad (68)$$

This implies that to obtain the electron scattering amplitude we must multiply (67) by $e^{-B\frac{\sin^2\theta}{\lambda^2}}$.

In Table VI we have written x-ray structure factors as determined by Uno [22], Togawa [23] and Sanger [24]. The corresponding values for U_{200} and U_{400} for 100 keV electrons and the accelerating voltage independent values of V_{200} and V_{400} have been determined using $B_{Mg} = 0.24\ \mathring{A}^2$, and $B_O = 0.19\ \mathring{A}^2$ for Togawa's and Uno's structure factors, and $B_{Mg} = 0.33\ \mathring{A}^2$, $B_O = 0.31\ \mathring{A}^2$ for Sanger's.

In Table VII we have given values of U_{200} and U_{400} at 100 keV, and the corresponding V_{200} and V_{400} for the theoretical free atom values of Table I reduced with $B = 0.26$ and for the structure factors of Tokonami-Yamashita, reduced with $B_{Mg} = 0.24\ \mathring{A}^2$ and $B_O = 0.19\ \mathring{A}^2$ (as taken from a table given by Miyake [25]).

Finally in Table VIII, we have given the x-ray values of Table VI, the theoretical values of Table VII and the experimental electron diffraction values of Goodman and Lehmpful [26] (GL in the future), D, UN, Moliere and Nihers [27], Moliere and Lehmpfuhl [28], and Cowley et al. [29], besides our best fitting values.

Next, we compare our results with all the other values in Table VIII.

TABLE VI (20°C)

	F_x (hkl)		U_{hkl} (Å^{-2})		V_{hkl} (volts)	
	200	400	200	400	200	400
Togawa	54.16	29.92	0.0532	0.0247	6.67	3.10
Uno	54.70	29.07	0.0521	0.0251	6.53	3.15
Sanger	54.06	29.06	0.0523	0.0242	6.56	3.04

TABLE VII

	U_{hkl} (Å^{-2})		V_{hkl} (volts)	
	200	400	200	400
Tokonami-Yamashita	0.0524	0.0247	6.57	3.11
Free Atom	0.0576	0.0249	7.27	3.13

TABLE VIII

		V_{200}	V_{400} (volts)	
X-ray	Togawa	6.67	3.10	
	Uno	6.53	3.15	
	Sanger	6.56	3.04	
Theory	Tok-Ya	6.57	3.11	
	Free atom	7.22	3.13	Temp. ~20°C
Electron Diffraction	Best fit	6.63	3.42	
	GL	6.92	----	
	D	7.64	----	
	UN	7.46	----	
	Mo-Ni	7.55	2.60	
	Mo-L	7.80	3.20	
	Cowley et al.	8.00	2.70	

First of all, we should compare our results with all the electron diffraction values in Table VIII. All the electron diffraction values with the exception of those of GL are clearly non-accurate. They were determined or by straight forward application of two beam theory to experimental extinction distances, or by neglecting relativistic effects, or by using Bethe's second approximation. GL have made short comments on these points. Nevertheless, they have not analyzed the failure of the two beam theory for MgO when considering results for the variation of ε_{200} with deviation from the Bragg peak. We shall devote later a section to analyze this failure, as the same confusing affirmations are done in paper after paper [30], [19] regarding its validity. The failure of Bethe's second approximation for MgO will also receive further comments.

As a consequence of the preceeding remarks, we shall compare our values with those of GL. The experiment of these authors is based in the method of convergent beam diffraction. The method provides a record of variation of intensities of all the diffracted beams with angle of incidence or primary beam for constant crystal thickness. Corresponding calculations are made on the basis of assumed values for the Fourier coefficients of the potential distribution (they do not mention their values), and these coefficients varied till they fit the intensities. No direct compariston of this method with ours seems possible. They affirm that their intensity patterns are not sensible to a fitting of U_{600}, but our

method is (see 5.1). Their final value of V_{200} (corresponding to $U_{200} = 0.0552$ $\mathring{A}^{-2}$ at 100 keV) seems much higher than ours.

Study of Table III indicates that for $\varepsilon_{200} = 456 \pm 10\mathring{A}$ at 100 keV their value could be in agreement with our fitted values with $\frac{\varepsilon_{400}}{\varepsilon_{200}} \simeq 5.9 \pm 8$. Nevertheless, no complete comparison can be made, as they do not give their fitted value for V_{400}.

Comparison with x-ray values should be more rewarding because this time we can compare V_{200} and V_{400}. At this point we should like to note that the value of V_{200} for Togawa listed in Table VIII is different from the one listed by GL*. Although they have given a value for 0°K, the reduced temperature corrected value, of the order of 6.8 Volts lies slightly far from our value of 6.67 Volts.

Although comparison of V_{200} shows reasonable agreement with x-ray values, the same thing cannot be said of V_{400} that is greater in our case.

X-ray values of U_{200}, U_{400}, U_{600} ... for Uno and Togawa's x-ray scattering factors at 100 keV as listed in Tables VI and IV have been substituted in the many beam matrix, and $\frac{\varepsilon_{400}}{\varepsilon_{200}}$ calculated. Corresponding values for other energies have also been calculated from 200 to 500 keV. The results have been plotted in figure 8.

At 100 keV for Togawa's and Uno's values, ε_{200} and $\frac{\varepsilon_{400}}{\varepsilon_{200}}$, where respectively ~458, ~466 $\mathring{A}$ and ~4.5, ~4.15

*The same thing happens with the value of Tokonami-Yamashita.

Both values of ε_{200} show very good agreement with the electron diffraction value of $\varepsilon_{200} = 456 \pm 10$ Å.

A study of Table III (taking into account the corrections to U_{200} and U_{400} cited below the table), shows that taking $\varepsilon_{200} = 456$, U_{400} agrees with Togawa's for $\frac{\varepsilon_{400}}{\varepsilon_{200}} \simeq 4.4$ giving us $U_{200} \simeq 0.0535$ Å^{-2} close indeed to Togawa's value. Thus, if an experimental value of 4.4 for $\frac{\varepsilon_{400}}{\varepsilon_{200}}$ was to be obtained at 100 keV for $\varepsilon_{200} = 456$ Å, the agreement between our fittings and the values of Togawa should be very good.

When comparison with theoretical values is done, it is seen (excluding the difference that once again appears for values of V_{400}) that the free atom value of V_{200} is much larger than ours, while Tokonami-Yamshita's lies closer. The values of $\frac{\varepsilon_{400}}{\varepsilon_{200}}$ for different energies in the free atom case have also been plotted in figure 8.

Let us come back now to the comparison with GL. This time we shall adopt $U_{400} = 0.0247$ Å^{-2} as the value that GL perhaps obtained, based on the fact that it is an average of x-ray values in Table VI. For $\varepsilon_{200} = 446$ Å and a fit of $\frac{\varepsilon_{400}}{\varepsilon_{200}} \simeq 4.7$ at 100 keV, Table III predicts a value $U_{200} \simeq 0.048$ Å^{-2} close to the result of GL (0.0552).

It is then concluded, that according to our fittings, some of the values for V_{200} and V_{400} given in preceeding investigations are plausible, if and only if experimental values for $\frac{\varepsilon_{400}}{\varepsilon_{200}}$ at 100 keV are obtained ranging between 4 and 5. This seems to be far from the value of 3.26 given by U, but in his own words, a large experimental error can be

expected because of the way in which thickness fringes spacings were measured.

We believe that it is important to repeat the experiments over the whole range of energies as, if in the case of good experimental conditions, values are close to those given by U for $\frac{\varepsilon_{400}}{\varepsilon_{200}}$ this means the failure of (68) to convert x-ray into electron diffraction data for temperatures different from 0°K, when a fitting of ε's is attempted.

If measurements are fine enough, it is possible that values of B for different experiments can be deduced as different values of B produce different curves in figure 8.

5.5 The Variation of ε_{200} with the Accelerating Voltage from 100 to 1000 keV.

It is interesting to study the variation of ε_{200} with different accelerating voltages from 100 to 1000 keV, as experimental results by D are available for comparison.

The results for D are given in figure 9 (circles). The lowest curve in the figure (---) corresponds to calculations performed with the theoretical values of Table I. Similar results were obtained by Goringe et al. [31]. They tried to explain the experimental results of D by many beam theory including a complex part in the crystal potential to account for absorption effects (see section 8). The coincidence of both, their calculation and ours (to 3Å at 500 keV) provides the basis to affirm that it is not important in our fitting method not to take complex crystal potentials into account.

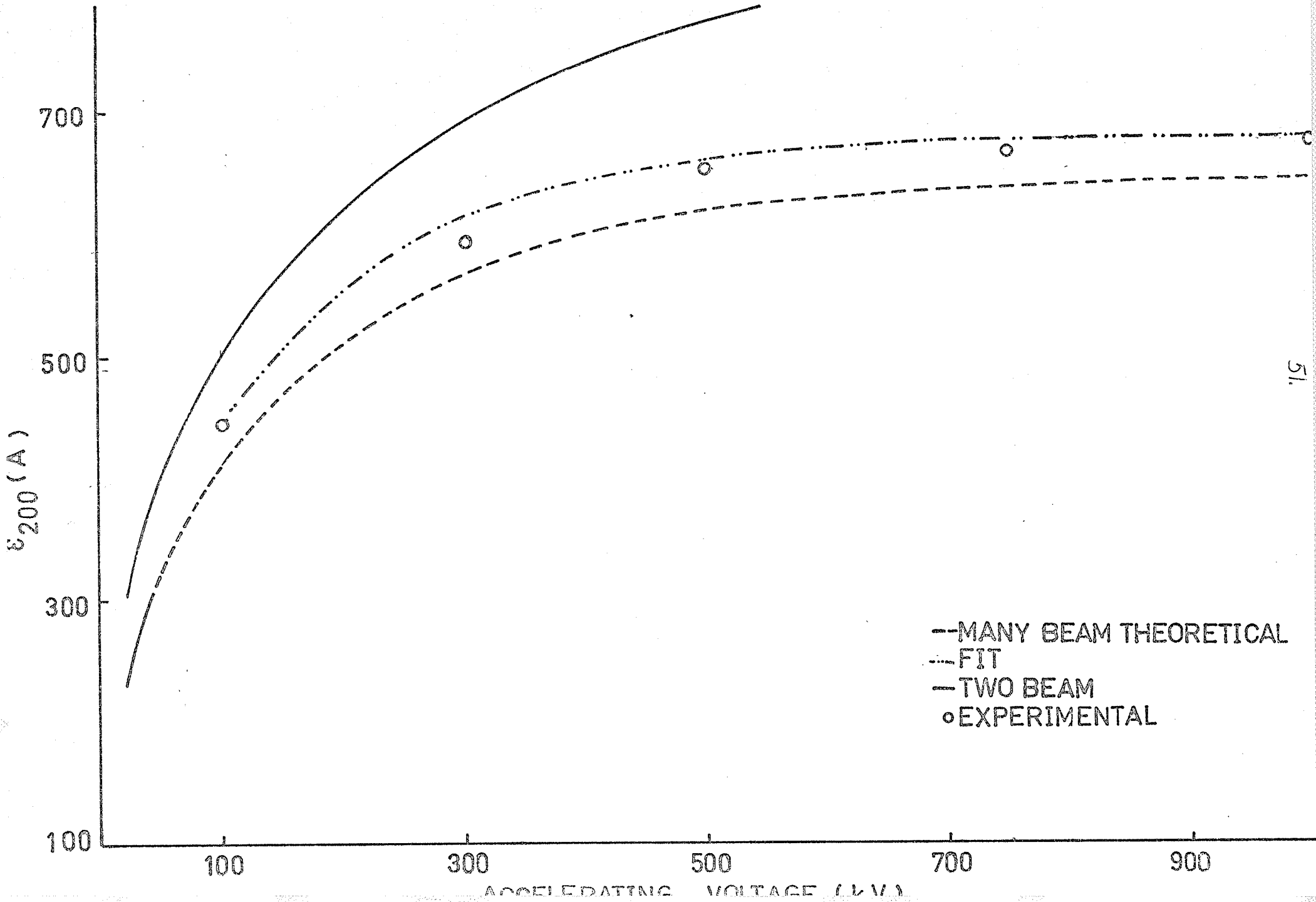
700
500
300
100
ε_{200} (A)
100
300
500
700
900
ACCELERATING VOLTAGE (kV)
MANY BEAM THEORETICAL
FIT
TWO BEAM
EXPERIMENTAL

The highest curve in figure 9 (———) corresponds to a two beam theory for $U_{200} = 0.0538$ Å^{-2} at 100 keV. Large differences with the experimental values and with the lowest curve are appreciable.

Finally we have plotted a curve (-·-·-) for $\varepsilon_{200} =$ 446 Å at 100 keV, with U_{200} and U_{400} as in Table III, 3.85 fit, and U_{600} , U_{800} , U_{1000} ... as in Table I.

Maximum deviations of the order of 12 Å are observed in relation with the experimental values of D, but these lie in the range of possible experimental error. It is possible that a more accurate fitting can be done if for the same value of ε_{200}= 446 Å at 100 keV, larger values of $\frac{\varepsilon_{400}}{\varepsilon_{200}}$ are adopted, but this has not been done by lack of experimental evidence for those values (see 5.4).

5.6 Determination of $\varepsilon_{200}(s)/\varepsilon_{200}$ for 100 keV Electrons. Conclusions on the Validity of a Two Beam Theory for MgO.

As we mentioned in 5.4, some of the electron diffraction data in Table VIII are given by applying two beam theory to experimental values of extinction distances. As a variation of ε_{200} with deviation from the Bragg condition seems to agree with the predictions of a two beam theory (see section 3), the formula (57):

$$U_{200} = \varepsilon_{200} K \qquad (57)$$

is used to transform experimental values of ε_{200} into values for the Fourier coefficient of the crystal potential.

In figure 10 we have plotted values of $\frac{\varepsilon_{200}(s)}{\varepsilon_{200}}$ at 100 keV for different deviations from the Bragg condition for the 200 reflection. When $\Delta\theta = \theta_{200}$ the 400 reflection is at the Bragg peak. When $\Delta\theta = 0$ the 200 reflection is at the Bragg peak.

We have plotted some experimental values by UN and U (circles), many beam values for the theoretical potentials of Table I (-·-), and many beam values for U_{200} and U_{400} corresponding to $\varepsilon_{200} = 456\text{Å}$ and $\varepsilon_{400}/\varepsilon_{200} = 3.85$ in Table III, and U_{600}, U_{800} ... as in Table VI (---). This last curve fits reasonably well the experimental data although perhaps a curve for a higher value of $\varepsilon_{400}/\varepsilon_{200}$ could give a slightly better fit.

The two beam curve for $U_{200} = 0.058\ \text{Å}^{-2}$ was seen to agree very well with (---). The only divergence appeared for values of $\Delta\theta/\theta_{200}$ greater than 0.8. It is likely that this fact led U and UN to the surprising affirmation of the validity of a two beam approach for 100 keV electrons.

Next a two beam curve for $U_{200} = 0.0537\ \text{Å}^{-2}$ was plotted (———), this potential was taken as a compromise between some of the experimental results available.

It is clear in the figure that this two beam curve lies far from the experimental values available, and as a consequence, it is concluded that a two beam theory is not explanatory of the variation of ε_{200} with deviation from the Bragg peak at 100 keV.

Figure 10. The variation of ε_{200} for 100 keV with deviation from the Bragg peak.

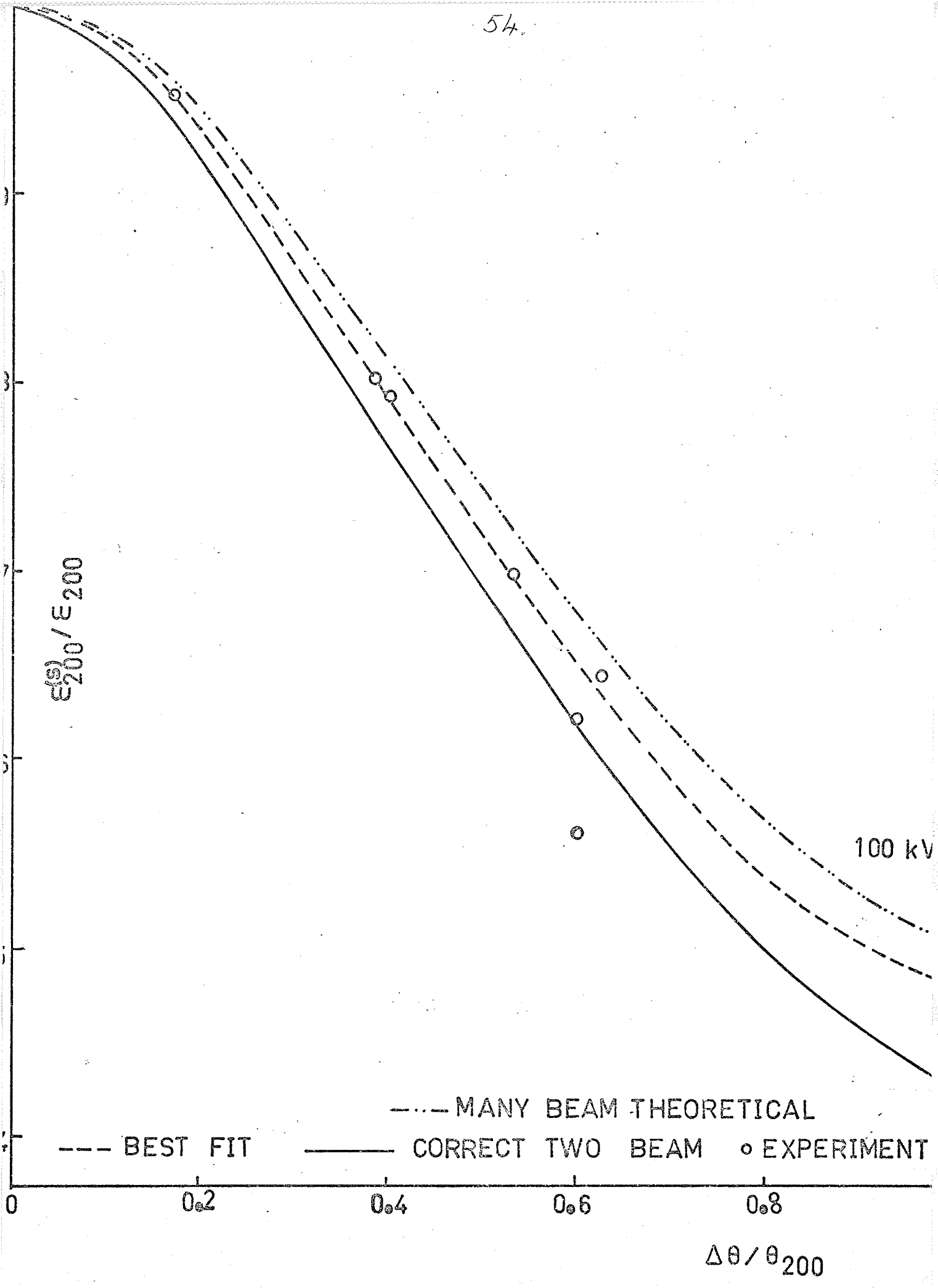
$\varepsilon^{(s)}_{200}/\varepsilon_{200}$
100 kV
MANY BEAM THEORETICAL
BEST FIT
CORRECT TWO BEAM
EXPERIMENT
0
0.2
0.4
0.6
0.8
$\Delta\theta/\theta_{200}$

5.7 Determination of $\varepsilon_{200}(s)/\varepsilon_{200}$ for $\Delta\theta = \theta_{200}$ for Different Accelerating Voltages from 100 to 500 keV.

When in figure 10, $\Delta\theta = \theta_{200}$ the 400 reflection is at the Bragg peak. Values for $\frac{\varepsilon_{200}(s)}{\varepsilon_{200}}$ with the 400 reflection at the Bragg peak have been plotted versus incident energy (from 100 to 500 keV) in figure 11. The circles are experimental points given by UN, and the curves MT, F and TR correspond to (-·-·-), (--) and (———) of figure 10.

Although F seems to give the best fit for the experimental values, the accuracy of the experimental points is not enough to draw definitive conclusions on the accuracy of F.

The lack of accuracy for the experimental points in figure 11 is due to the way in which they are measured, by direct measurements on thickness fringes photographs. This could obviously be corrected in future experiments.

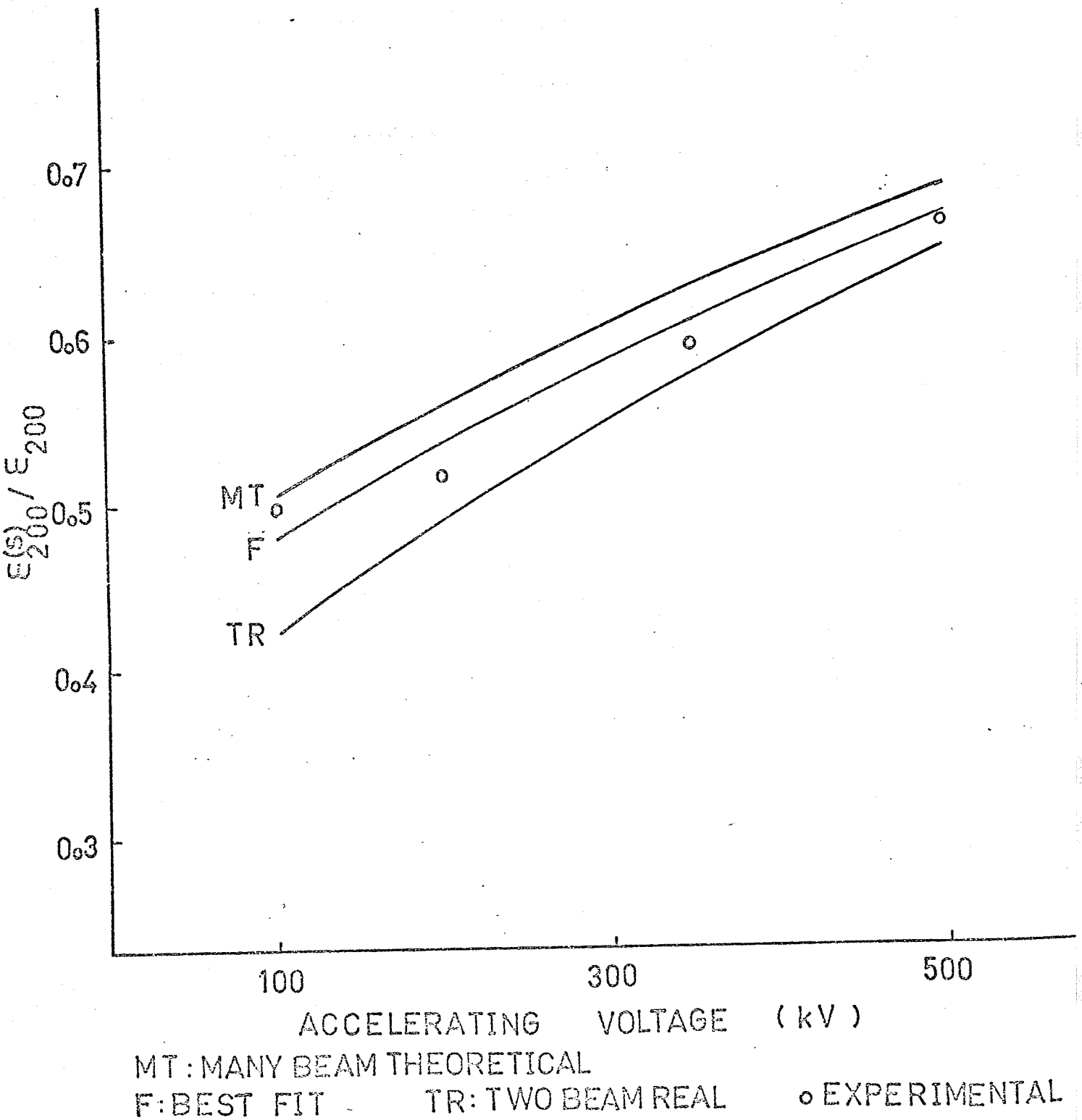

MT : MANY BEAM THEORETICAL
F : BEST FIT TR : TWO BEAM REAL o EXPERIMENTAL

CHAPTER VI

6.1 The Second Approximation of Bethe. Validity of its Use for MgO.

The second approximation of Bethe states that to take many beam effects into account in the two beam theory, a modification of the two beam relativistic potential must be written, if only systematic reflections are taken into account, in the form [19]

$$U^1(h) = U(h) - d^2 \sum_{h_1}'' \frac{U(h_1)\, U(h-h_1)}{h_1\,(h-h_1)} = U(h) - B(h) \qquad (69)$$

where d is the spacing of the first order reflection, and Σ'' means summation over positive and negative integers except for h and zero. $B(h)$ is usually appreciable for the second order reflection of a strongest first order reflection, and often amounts to more than one third of $U(h)$.

Generally, only a few terms in the expansion have importance. In fact, as tested by the author, the fifth crystal potential for example, can be made equal to zero without any appreciable change in the results, and the same happens with higher order potentials. This does not take place in a many beam theory where some results are sensible to the inclusion of more than four potentials.

In a two beam theory

$$\frac{U_{400}}{U_{200}} = \frac{\varepsilon_{200}}{\varepsilon_{400}} \qquad (70)$$

and in Bethe's approach

$$\frac{U'_{400}}{U'_{200}} = \frac{\varepsilon_{200}}{\varepsilon_{400}} \qquad (71)$$

In his paper, U, convinced of the general success of equation (71) tried to explain his experimental measurements (circles in figure 8) to (71) by assuming them in the necessary error.

His curve for $\frac{\varepsilon_{400}}{\varepsilon_{200}}$ lies in figure 8 almost coincident with our 3.26 fit, but it seems that he chose to calculate it a value for U_{200} of 0.051 $\mathring{A}^{-2}$ at 100 keV, that lies far from our fits and other available values. He does not explain the reason for his selection. At this point, it seemed interesting to derive Bethe's U'_{200} and U'_{400} and to see the correspondence with many beam results.

The expansion of U'_{400} gives

$$U'_{400} = U_{400} - d^2 \{U^2_{200} - \frac{2}{3} U_{200} U_{600} - \frac{2}{8} U_{400} U_{800} - \frac{2}{15} U_{600} U_{1000} \ldots\} \quad (72)$$

We have plotted in figure 12 U'_{400} from computations with the potentials of Table I (and the corresponding values for 200 ...900 ...1200 keV) (-·-) and for values corresponding to (--) in figure 10 and U_{600} , ... as in Table I*. These are called in the figure T and F respectively. It is interesting to observe how different are the voltages for which the potential U'_{400} becomes zero (the value of U_{200} is seen to have a great importance in equation (72) through the term in U^2_{200}).

Next U' was computed from the expression

$$U'_{200} = U_{200} - d^2 \{U_{200} U_{400} - \frac{1}{3} U_{400} U_{600} - \frac{1}{6} U_{600} U_{800} \ldots\} \quad (73)$$

---

*At this point we did not correct U_{600} ... for temperature.

Figure 12. The variation of Bethe's U'_{00} with accelerating voltage from 100 to 1200 keV.

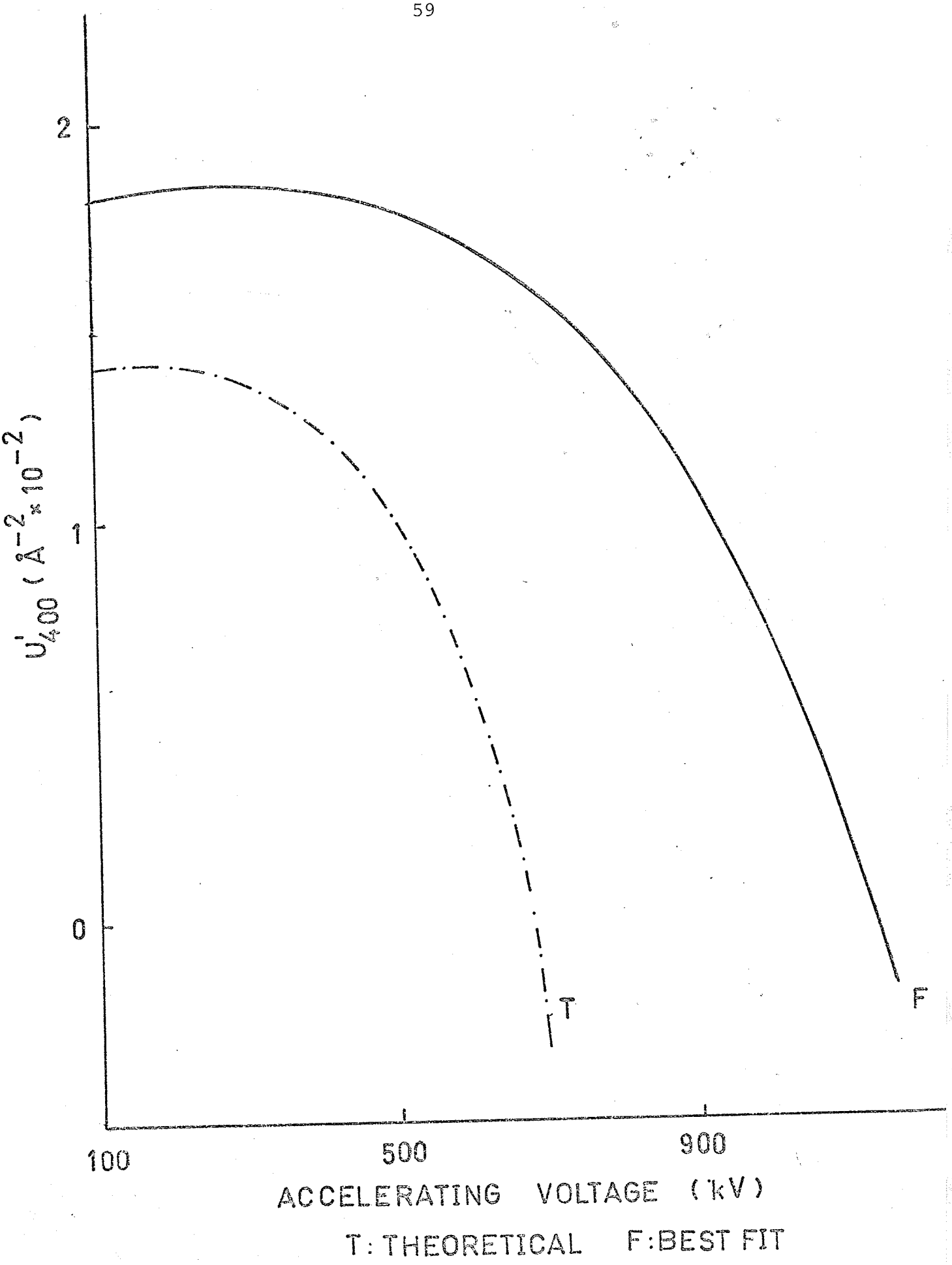
2
1
0
U'_{400} ($Å^{-2} * 10^{-2}$)
T
F
100
500
900
ACCELERATING VOLTAGE (kV)
T: THEORETICAL F: BEST FIT

and the ratios obtained $\frac{\varepsilon_{400}}{\varepsilon_{200}}$ were compared with the corresponding many beam results for T and F. A difference of 0.4 was observed between the values of $\frac{\varepsilon_{400}}{\varepsilon_{200}}$ for T at 100 keV, as obtained by many beam and Bethe's theory, but when comparison was made at 500 keV the difference was of the order of ~3.2. Less important differences were observed for the values of the Fourier coefficients corresponding to F.

It is clear, that Bethe's second approximation does not provide in the case of MgO, sufficient explanation for the many beam values of $\frac{\varepsilon_{400}}{\varepsilon_{200}}$.

Recently, Cowley [32] formulated Bethe's second approximation as a particular case of a more general formula, guided by the fact that the approximation seems to be successful sometimes to account for the extinction of second order Kikuchi lines [33], [34], [35] in some materials. For thick crystals, electrons forming Kikuchi lines have undergone, on the average, a large number of inelastic and elastic scattering processes so that the Kikuchi line intensity may be considered as given by the incoherent addition of electron beams originating from various depths in the crystal.

Thus, to a good approximation (following Cowley)

$$I(h) = \int_0^\infty |T_1(h)+T_2(h) + \ldots|^2 \, dt \qquad (74)$$

where t is the crystal thickness, and T(h) represent the contribution of the beams scattered once, twice, etc. He obtains a general expression for I(h) of the type

$$I(h) = \alpha\left[U(h)-d^2 \sum_{h_1} \frac{U(h_1)U(h-h_1)}{h_1(h-h_1)} + d^4 \sum_{h_1 h_2} \sum \frac{U(h_1)U(h_2)U(h-h_1h_2)}{h_1(h-h_1)(h_1-h_2)(h-h_1h_2)}\right] \qquad (75)$$

of which the first two terms are identical with (69).

Equation (75) has been used in an attempt to obtain a better agreement of the new $\frac{\varepsilon_{400}}{\varepsilon_{200}}$ with the many beam results corresponding to T and F. No significant improvement has been obtained in the preliminary calculations. It has been seen that the influence of the new terms is always positive for U'_{200}, and thus, larger values than for the original second approximation (69) are obtained. The increase is, nevertheless, only of the order of 10^{-3} $\mathring{A}^{-2}$ for 500 keV. The influence of the new terms in U'_{400} is different, as both new positive and negative terms have to be taken into account. It is seen to be of the order of $10^{-4}\mathring{A}^{-2}$ at 300 keV.

In a recent paper, Cowley and Turner [36] have applied equations of similar structure to (75) for electron structure analysis of policrystalline materials. Agreement with our findings may lie in the fact that they are not able to fit the experimental data.

CHAPTER VII

7.1 The Determination of V_{111} and V_{222} for Si.

Special interest lies in the determination of the scattering factor for the 222 theoretically forbidden reflexion in Si, as Pollard and Turner [16] have found by a non-systematic intensity fitting method, values for V_{111} and V_{222} very different from the x-ray values of different authors.

Sheinin and Cann [37] have found at 151 keV a value for the extinction distance for the 111 reflection of 840± 40 Å. On the other hand, in his report of Pollard and Turner's work, Cowley [32] has shown a microdensitometer plot that, amplified, has allowed us to determine the correspondent extinction distance $\varepsilon_{222} \simeq 1670$ Å. Dr. Cowley [38] has pointed out to us that the plots were obtained at 100 keV.

Referred to a face centered cubic lattice, the basis of Silicon is (000) (¼, ¼, ¼). Thus, if fcc represents the structure factor for a face centered cubic lattice

$$F_\theta^{(hkl)} = [f.c.c]\ [\exp\ (-2\pi\ (\tfrac{h}{4}+\tfrac{k}{4}+\tfrac{l}{4}))+ 1] \qquad (76)$$

With the object of determining the signs of the structure factors for the 111 set of systematic reflections considered, we take as new basis (±1/8, ±1/8, ±1/8) and obtain

$$F_\theta^{(hkl)} = 2[f.c.c]\ [\cos\ 2\pi(\tfrac{h}{8}+\tfrac{k}{8}+\tfrac{l}{8})] \qquad (77)$$

The existance of the (222) reflection, forbidden by (77) can be elementarily justified by admitting the existance

of an extra concentration of electrons midway between the two nearest neighbours Si atoms.

With a value of $B = 0.22$ in equation (68) and theoretical values for the electron scattering amplitudes $f_\theta(hkl)$ at 0°K as in Table IX, theoretical Fourier coefficients of the crystal potential were obtained at 20°C by (64) and are also listed in the same table with their respective signs.

Values in the table are as in all the tables in the thesis at 100 keV. Values for 151 keV are immediately obtainable from them, by taking at 151 keV $K = 33.83$ Å^{-1} and $\sqrt{1-\frac{v^2}{c^2}} = 0.773$.

TABLE IX

$g = 0.3189$ Å^{-1}

	111	222	333	444	555	666	777
f_θ	3.242	0	0.788	0.535	0.382	0	0.230
U_{hkl}	-0.0433	0	+0.0104	-0.0093	+0.0045	0	-0.0021

Application of the fitting method for $\varepsilon_{111} = 840 \pm 40$ Å at 151 keV, and $\varepsilon_{222} = 1754$ Å at 100 keV, gave results for U_{111} and U_{222} that are written at 100 keV in Table X, where we also give the values of U_{111} and U_{222} resulting from an average of structure factors of different authors with $B = 0.22$ [40], and the values obtained by Pollard and Turner.

In the table, we see that both x-ray values lie in the range of our fittings. Nevertheless, if we take the x-ray

value for U_{222} as $0.0008\,\text{Å}^{-2}$ correspondence with the electron.

TABLE X

		Fit	Pollard Turner	X-ray	
100 keV	U_{111}	-0.0395 ± 0.0020	0.0417	0.0038	Å^{-2}
	U_{222}	-0.0001 ± 0.0012 [5]	0.000028	0.0008	

diffraction value is found at $\varepsilon_{111} \simeq 813$ Å (151 keV), that lies far from $\varepsilon_{111} = 840$ Å (at 151 keV). On the other hand, if we take the x-ray value $U_{222} = -0.0008\ \text{Å}^{-2}$ (at 100 keV). This corresponds in our fittings to $\varepsilon_{111} \simeq 866$ Å (at 151 keV) at a value of $U_{111} \simeq -0.0384\ \text{Å}^{-2}$ (at 100 keV) very close to the x-ray value $U_{111} = -0.038\ \text{Å}^{-2}$ (at 100 keV).

Nevertheless, in all the manipulations of the x-ray data [39], [40] the sign for F_x (111) is different from the sign for F_x (222) and so, the signs - and + should be considered for U_{111} and U_{222} respectively and $\varepsilon_{111} \simeq 813$ Å taken (at 151 keV) as best value for ε_{111}, if the signs of U_{111} and U_{222} obtained by our fitting method were to agree with the signs attributed to the x-ray values.

Unfortunately, definitive conclusions cannot be attempted because the error in the experimental extinction distance of Cann and Sheinin is too large (they have used an experimental method more inaccurate than the one used by D and UN), and it is also possible that some error exists in the value taken for ε_{222}, as reported to us by Dr. Turner [41] in a recent private communication. It seems that as in

the case of MgO, values of $\frac{\varepsilon_{222}}{\varepsilon_{111}}$ at voltages from 100 to 500 keV should be required before any definitive conclusions on the absolute values of V_{111} and V_{222} are reached.

CHAPTER VIII

8.1 The Inclusion of Absorption Effects in the Dynamical Theory.

Experimental observations of thickness fringes on electron micrographs do not conform exactly to the predicted profiles (see sections 3 and 4). Instead of uniformity in tense fringes, the fringe intensity decreases rapidly and differently for different materials, with crystal thickness.

Frequently only about four to six fringes can be seen even though appreciable intensity can be transmitted and diffracted when the crystal has over twice this thickness. In two beam theory, we saw in Chapter III, that one of the Bloch waves excited in the crystal spends more time than the other in a region of low potential energy, near the atoms in the crystal; that is, it is more scattered than the other wave.

The most reasonable explanation of the absorption effect is that the wave that is more scattered is in fact scattered outside the aperture of the objective in the electron microscope, and thus appears to be effectively absorbed. Thickness fringes would occur only when the waves have a comparable intensity, that is for thin crystals.

In the general many beam case, absorption of the incident electrons is treated phenomenologically by adding a small imaginary part $V'(\vec{r})$ as a perturbation to the crystal potential $V(\vec{r})$. The result of using the complex crystal

potential $iV'(\vec{r}) + V(\vec{r})$ is that the intensity of the Bloch wave corresponding to the ith branch of the dispersion surface is multiplied by the attenuation factor $e^{-\mu(i)z}$ where z is the depth in the crystal and $\mu^{(i)}$ the absorption coefficient for the branch i. Assuming the Bloch wave to be normalized, use of perturbation theory to first order shows that

$$\mu^{(i)} = \frac{4\pi}{h^2 \vec{k}_z^{(i)}} \int \psi^{(i)*} V'(\vec{r}) \psi^{(i)} dz \qquad (78)$$

where

$$\psi^{(i)}(r) = \sum_G C_G^{(i)}(\vec{k}^{(i)}) \exp i (\vec{k}^{(i)} + \vec{G})\vec{r} \qquad (79)$$

The absorption coefficients $^{(i)}$ can be evaluated if it is assumed that $V'(r)$ has the periodicity of $V(r)$ since this allows expansion of $V'(r)$ in the form

$$V'(\vec{r}) = \sum_G V'_G \exp(i\vec{G}\cdot\vec{r}) = \frac{h^2}{2me} U'_G \exp(i\vec{G}\vec{r}) \qquad (80)$$

Use of the approximation $k^{(i)} \simeq K$ and substitution of (80) into (78) shows that

$$\mu^{(i)} = \frac{2\pi}{K} \sum_G \sum_h U'_{G-h} C_h^{(i)} C_G^{(i)*} \qquad (81)$$

In general, the addition of the complex term to the real crystal potential may cause an addition to the real part of the extinction distance of Chapter VI as well as the existence of a new imaginary part. Nevertheless, following section 5.5, it does not seem that the consideration of a complex crystal potential plays an important role, if any, in the results of our fitting method.

CHAPTER IX

9.1 Description of the Results Obtained in the Search for a Method of Fabricating Wedge Crystals of Copper by Evaporation.

The new interest aroused in the possible accuracy of scattering factors as determined by the method used in Chapters V and VII, strongly suggested the importance of extending the determination of extinction distances to more materials than MgO and Si. Mathews [42] mentions the formation of wedge crystals of gold in the process of studying some nucleation processes, by evaporating the metal on hot substrates of ClNa at ultrahigh vacuum (10^{-8}mm).

A NRC high vacuum equipment was used to evaporate copper of 99.9% purity in hot ClNa and KBr substrates with a final vacuum of the order of 10^{-6}mm when evaporation took place. Ino [43] has reported single crystal growth for ultrahigh vacuum pressures ($<10^{-6}$mm) and 95% single crystal growth for pressures $>10^{-6}$mm, when the substrate is kept at temperatures between 300 and 400 Centigrade. In nucleation theory, two important parameters regulate the degree of epitaxy of a film: the temperature of the substrate, and the rate of evaporation [44]. It is merely a question of patience to find the best experimental conditions for the material in question.

To grow a wedge crystal, it is necessary to devise some specific arrangement inside the high vacuum chamber. We adopted a non-movable shutter that was placed at distances from

one to three mm from the crystal surface, and at ten cm or less from the evaporator. The temperature of the substrate was measured with a thermocouple and was kept constant for 360°C in the whole experiment. Great difficulty was found in reproducing experimental conditions. Observations were made with a Philips EM 300 electron microscope.

During the two months of experiment only two 95% epitaxial films were obtained, but in these, as in all the others, bend contours were completely unavoidable, and thickness fringes were never seen.

The analysis of bend contours by electron diffraction theory is full of uncertainties (compare for example the different extinction voltages found for aluminum by different workers* [45], [35]) and no conclusions were drawn from the experimental results.

*Extinction voltage is the voltage for which U'_{222}, as calculated by Bethe's second approximation, is zero.

CONCLUSIONS AND SUGGESTIONS FOR FURTHER RESEARCH

In this thesis, we have reached the following conclusions:

(1) The systematic fitting method developed indicates for MgO that many of the available results for V_{200} are plausible if and only if, for 100 keV, experimental values for $\varepsilon_{400}/\varepsilon_{200}$ are obtained between four and five, if (38) can be used when fitting ε's.

(2) The two beam theory and Bethe's second approximation are not applicable to the study of the {2,0,0} set of systematic reflections of MgO in spite of some affirmations to this respect.

(3) No definitive conclusions can be reached for the sign of V_{222} in Si, but in the fittings attempted, V_{111} is far from the free atom value.

Preceeding conclusions show that new experimental values of low order extinction distances are necessary for both MgO and Si, and that accuracy in these experiments is very important. In particular, measurements of extinction distances should be done taking the positions of the intensity minimae (see section 4.2). At the same time, new methods to fabricate wedge crystals for common metals should be devised.

APPENDIX

APPENDIX I

Determination of the Relation Between Fourier Coefficients of the Crystal Potential and Electron Structure Factors.

Let us suppose an electron incident in a crystal with wave vector K_o and velocity $\vec{v}$. Let the incident energy be eE and the work function of the material be $-eV_o$.

The equation

$$\frac{1}{2}m\vec{v}^2 = eE + eV_o \tag{82}$$

or its equivalent

$$m^2v^2 = 2m\ (E + V_o) = h^2K^2 \tag{83}$$

where K_o inside of the crystal is K, are obvious. Thus

$$\frac{K}{K_o} = \left(\frac{E + V_o}{E}\right)^{\frac{1}{2}} \tag{84}$$

and if $V_o << E$

$$\frac{K}{K_o} = 1 + \frac{V_o}{2E} \tag{85}$$

where K/K_o can be defined as a mean refractive indix. If $\Delta K = K - K_o$

$$\frac{\Delta K}{K_o} = \frac{1}{2}\frac{V_o}{E} \tag{86}$$

Let us now suppose an incident plane wave

$$\psi_o\ e^{2\pi i\ \vec{K}_o\vec{r}} \tag{87}$$

The amplitude of the scattered wave at a distance x ahead is

$$f_\theta\ \frac{e^{2\pi i\ \vec{K}_o\vec{r}}}{\vec{r}}\ \psi_o \tag{88}$$

where f_θ is the electron scattering factor.

The reflected wave can be thought of as arising from the superposition on an incident plane wave and a scattered plane wave 90 degrees out of phase. To find the disturbance at a point P, ahead of the wave front, the standard procedure is to divide the plane at a distance r from P into Fresnel zones, where the edges of the zone are at distances $r + \lambda/2$, $r + \lambda$ etc. from P. It is possible to find out that the total disturbance at P is equal to half of the contribution due to the first zone of radius $R = \sqrt{\lambda r}$. The amplitude scattered by a foil of thickness dz is

$$d\psi_s = \frac{i}{\pi} \pi R^2 f(\theta)\ dr\ \frac{e^{2\pi i\ \vec{K}\vec{r}}}{\vec{r}}\ \psi_o \qquad (89)$$

Substituting for R, and if the amplitude of the scattered wave is very small (Born approximation) we obtain

$$\psi = \psi_o\ e^{2\pi i\ (K_o + \frac{\lambda f}{2\pi})\vec{r}} \qquad (90)$$

where $\frac{\lambda f}{2\pi}$ corresponds to ΔK in (86). Thus

$$f = \frac{2\pi m_o e}{h^2} V \qquad (91)$$

These considerations are valid for the amplitude scattered from a unit volume. The volume dz gives rise to the scattered amplitude

$$\psi_o\ \frac{2\pi m_o e V}{h^2}\quad \frac{e^{2\pi i\ \vec{K}_o\vec{r}}}{r}\ dz \qquad (92)$$

The amplitude of the scattered wave by a unit cell at a point P at a distance r_i from the origin will be

$$\psi_s = \frac{2\pi m_o e}{h^2} \int_{\text{unit cell}} V(\vec{r}_i)\ \frac{e^{2\pi i\ \vec{K}_o|\vec{r}-\vec{r}_i|}}{|r-r_i|}\ e^{2\pi i\ \vec{K}_o\vec{r}_i}\ dz_i \qquad (93)$$

where $V(\vec{r}_i)$ is the potential at a point $\vec{r}_i$ and we have made $\psi_o = 1$.

If $|\vec{r}|$, $|\vec{r}-\vec{r}_i| >> |\vec{r}_i|$, we can replace $|r-r_i|$ in the denominator by $|r|$ in the denominator and by $r-\frac{\vec{K}\vec{r}_i}{K}$ in the expotential, where K is the wave vector of the scatter wave and $|K| = |K_o|$ outside of the crystal to a very good approximation. Hence

$$\psi_s = \frac{2\pi m_o e}{h^2} \frac{e^{2\pi i \vec{K}_o \vec{r}}}{r} \int V(r_i) e^{2\pi i (\vec{K}_o - \vec{K})\vec{r}} dz_i \qquad (94)$$

On the other hand, the amplitude scattered by the unit cell is

$$\psi_s = \frac{e^{2\pi i \vec{K}_o \vec{r}}}{r} \Sigma f_i(\theta) e^{-2\pi i |\vec{K}_o - \vec{K}| r_i} = \frac{e^{2\pi i \vec{K}_o \vec{r}}}{r} F_\theta \qquad (95)$$

where $f_i(\theta)$ is the scattering amplitude for one atom, and F_θ the electron structure factor. As a consequence

$$F_\theta = \frac{2\pi m_o e}{h^2} \frac{1}{V_c} \int V(r_i) e^{-2\pi i (\vec{K}_o - \vec{K})\vec{r}_i} dz_i \qquad (96)$$

where is the volume of the unit cell.

Since we are interested in the values of the Fourier coefficients of the crystal potential, we write

$$F_{hkl} = \frac{2\pi m_o e}{h^2 V_c} V_{hkl} \qquad (63)$$

APPENDIX II

In this appendix we present the two computer programs used throughout the thesis. The first calculates dispersion surfaces, the second extinction distances for variations of a determined Fourier coefficient of the crystal potential.

The subroutine used with the program was the subroutine eigen of the scientific subroutine package (in double precision). This subroutine only allows real Fourier coefficients as input. The inclusion of a complex crystal potential could be done with a new subroutine by Gibbs, recently available from IBM (August, 1969).

(749)

```
      DIMENSION A(81),B(81),P(81)
      DOUBLE PRECISION A,B,SE,SI,SOL,SO,SR,SP,SG,SZ,SV,SS,SL,SA,SH,R
      INTEGER H,V,U,P
      READ (5,10) (A(I),I=1,45)
      H=0
   10 FORMAT (F12.8)
    8 WRITE (6,91) A
   91 FORMAT (' ','ORIGINAL MATRIX'/(' ',8F11.5))
      DO 11 I=1,45
   11 B(I)=A(I)
      CALL EIGEN (A,R,9,0)
   20 FORMAT ('0 A='/(' ',8F14.7))
    9 WRITE (6,20) A
      WRITE (6,20) R
   23 SE=DSQRT(A(1))
      SI=DSQRT(A(3))
      SOL=DSQRT(A(1))-DSQRT(A(3))
      SO=SOL**(-1)
      SA=-DSQRT(A(3))-DSQRT(A(6))
      SH=SA**(-1)
      SR=DSQRT(A(6))
      SP=DSQRT(A(10))
      SG=DSQRT(A(15))
      SZ=DSQRT(A(21))
      SV=DSQRT(A(28))
      SS=DSQRT(A(36))
      SL=DSQRT(A(45))
      WRITE (6,200) SE,SI,SOL,SO,SR,SA
      WRITE (6,300) SP,SG,SZ,SV,SS,SL
      WRITE (6,400) SH
  200 FORMAT ('0',6G19.10)
  300 FORMAT ('0',6G19.10)
  400 FORMAT ('0',G19.10)
      N=0
      B(5)=B(5)-0.0001
      B(7)=B(7)-0.0001
      B(11)=B(11)-0.0001
      B(17)=B(17)-0.0001
      B(24)=B(24)-0.0001
      B(32)=B(32)-0.0001
      B(41)=B(41)-0.0001
      WRITE (6,10) B(5)
   19 DO 17 I=1,45
   17 A(I)=B(I)
      N=N+1
      IF (N-2) 8,8,30
   30 CALL EXIT
      END
```

(746)

```
      DIMENSION A(45),B(45),R(31)
      DOUBLE PRECISION A,B,SE,SI,SDL,SD,SR,SP,SG,SZ,SV,SS,SL,SA,SH,R
      INTEGER H,V,U,P
      READ (5,10) (A(I),I=1,45)
      H=0
   10 FORMAT (F12.3)
    8 WRITE (6,91) A
   91 FORMAT (' ','ORIGINAL MATRIX'/(' ',8F11.5))
      DO 11 I=1,45
   11 B(I)=A(I)
      CALL EIGEN (A,R,9,0)
   20 FORMAT ('0 A='/(' ',8E14.7))
    3 WRITE (6,20) A
      WRITE (6,20) R
   23 SE=DSQRT(A(1))
      SI=DSQRT(A(3))
      SDL=DSQRT(A(1))-DSQRT(A(3))
      SD=SDL**(-1)
      SA= DSQRT(A(3))-DSQRT(A(6))
       SH=SA**(-1)
      SR=DSQRT(A(6))
      SP=DSQRT(A(10))
      SG=DSQRT(A(15))
      SZ=DSQRT(A(21))
      SV=DSQRT(A(28))
      SS=DSQRT(A(36))
      SL=DSQRT(A(45))
      WRITE (6,200) SE,SI,SDL,SD,SR,SA
      WRITE (6,300) SP,SG,SZ,SV,SS,SL
      WRITE (6,400) SH
  200 FORMAT ('0',6G19.10)
  300 FORMAT ('0',6G19.10)
  400 FORMAT ('0',G19.10)
      N=0
       D=0.476/25
      V=0
      DO 39 J=1,17,4
      I=J-1
      V=V+I+1
      B(V)=729-B(V)
       B(V)=B(V)-2*D*DSQRT(B(V))+D**2
   39 B(V)=729-B(V)
        V=0
       DO 40 J=1,13,4
      I=J-1
      V=V+I+3
      B(V)=729-B(V)
       B(V)=B(V)+2*D*DSQRT(B(V))+D**2
   40 B(V)=729-B(V)
      N=N+1
      IF (N-16) 19,19,30
   19 DO 17 I=1,45
   17   A(I)=B(I)
      H=H+1
      IF (H-15) 8,8,30
   30 CALL EXIT
      END
```

REFERENCES

1. H.A. Bethe. (1928). Ann. Phys., 87, 55.

2. P.P. Ewald. (1916). Ann. Phys., 49, 1 and 49, 117.

3. M.V. Laue. (1931). Ergebnisse d. exacten Naturwiss, 10, 133.

4. S.L. Cundy et al (1969). Phil. Mag., 20, 147.

5. K. Fujiwara. (1962). J. Phys. Soc., Japan, 16, 2226 and 17 (sup. BII) 118.

6. R.M. Stern et al. (1969). Reviews of Modern Physics, 41, 275.

7. F. Fujimoto. (1959). J. Phys. Soc., Japan, 14, 1558.

8. A.J.F. Metherell and R.M. Fisher. (1969). Phys. Stat. Sol., 32, 551.

9. P.B. Hirsch et al. (1965). Electron Microscopy of Thin Crystals, London, Butterworths.

10. A. Howie and M.J. Whelan. (1961). Proc. European Conf. on E. Microsc., 1, 181. Delft, de Nederlandse Vereuiging vor Electroken microscopie.

11. A. Fukuhara. (1966). J. Phys. Soc. Japan, 21, 2645.

12. A. Howie. (1966). Phil. Mag., 14, 223.

13. A. Howie and S.A. Basinski. (1968). Phil. Mag., 17, 1039.

14. R. Sernells and R. Gevers. (1969). Phys. Stat. Sol., 33, 703.

15. R.W. James. (1965). The Optical Principles of the Diffraction of X-rays. Cornell University Press.

16. Reviewed in 32

17. R. Uyeda and M. Nonoyama. (1965). Jap. J. of Appl. Phys., 4, 498.

18. G. Dupoy et al. (1965). J. Microsc., 4, 429.

19. R. Uyeda. (1968). Acta. Cryst., A24, 175.

20. J.A. Ibers and B.K. Vainshtein. (1962). International Crystallographic Tables, Vol. III, Kynoch Press, Birmingham.

21. Y.H. Ohtsuki. (1966). J. Phys. Soc., Japan, 21, 2300.

22. R. Uno. (1963-1967). Unpublished, cited in 25.

23. S. Togawa. (1965). J. Phys. Soc., Japan, 20, 742.

24. P.L. Sanger. (1969). Acta. Cryst., A25, 694.

25. S. Miyake. (1969). Acta. Cryst., A25, 257.

26. P. Goodman and G. Lehmpfuhl. (1967). Acta. Cryst., A22, 14.

27. K. Moliere and H. Nihers. (1955). Zeit. Phys., 140,581.

28. K. Moliere and G. Lehmpfuhl. (1961). Zeit. Phys., 164, 389.

29. J.M. Cowley, et al. (1957). Acta. Cryst., 10, 19.

30. G. Jeschke and H. Niedrig. (1970). Acta. Cryst, A26, 114.

31. M.J. Goringe et al. (1966). Phil. Mag., 14, 217.

32. J.M. Cowley. (1969). Acta. Cryst., A25, 129.

33. S. Kikuchi. (1928). Jap. J. Phys., 5, 83.

34. D. Watanabe et al. (1968). Acta. Cryst., A24, 249.

35. D. Watanabe et al. (1968). Acta. Cryst, A24, 580.

36. J.M. Cowley and P.S. Turner. (1969). Acta. Cryst., A25, 450.

37. S.S. Sheinin. (1966). Phys. Stat. Solidi., 17, K143.

38. J.M. Cowley. (1970). Private communication.

39. B. Dawson. (1967). Proc. Royal. Soc., 298A, 379.

40. J.F. McConnell and P.L. Sanger. (1970). Acta. Cryst., A26, 83.

41. P.S. Turner. (1970). Private communication.

42. J. Matthews. (1966). Journal Vacuum Sci. and Tech., 3, 133.

43. S. Ino et al. (1964). Jour. Phys. Soc., Japan, 19, 881.

44. J.L. Kenty and J.P. Hirth. (1969). Surface Science, 15, 403.

45. F. Nagate and A. Fukuhara. (1967). Jap. Jour. Appl. Phys., 6, 1233.

46. G. Radi. (1970). Acta. Cryst., A26, 41.